# Evaluating effective reaction rates of kinetically driven solutes in large-scale, statistically anisotropic media: Human health risk implications

Erica R. Siirila[1,2] and Reed M. Maxwell[1,2,3]

Received 17 October 2011; revised 20 January 2012; accepted 7 March 2012; published 25 April 2012.

[1] The interplay between regions of high and low hydraulic conductivity, degree of aquifer stratification, and rate-dependent geochemical reactions in heterogeneous flow fields is investigated, focusing on impacts of kinetic sorption and local dispersion on plume retardation and channeling. Human health risk is used as an endpoint for comparison via a nested Monte Carlo scheme, explicitly considering joint uncertainty and variability. Kinetic sorption is simulated with finely resolved, large-scale domains to identify hydrogeologic conditions where reactions are either rate limited (nonreactive), in equilibrium (linear equilibrium assumption is appropriate), or are sensitive to time-dependent kinetic reactions. By utilizing stochastic ensembles, effective equilibrium conditions are examined, in addition to parameter interplay. In particular, the effects of preferential flow pathways and solute mixing at the field-scale (marcrodispersion) and subgrid (local dispersion, LD) are examined for varying degrees of stratification and regional groundwater velocities ($v$). Results show effective reaction rates of kinetic ensembles with the inclusion of LD yield disequilibrium transport, even for averaged (or global) Damköholer numbers associated with equilibrium transport. Solute behavior includes an additive tailing effect, a retarded peak time, and results in an increased cancer risk. The inclusion of LD for nonreactive solutes in highly anisotropic media results in either induced solute retardation or acceleration, a new finding given that LD has previously been shown to affect only the concentration variance. The distribution, magnitude, and associated uncertainty of cancer risk are controlled by the up scaling of these small-scale processes, but are strongly dependent on $v$ and the source term.

**Citation:** Siirila, E. R., and R. M. Maxwell (2012), Evaluating effective reaction rates of kinetically driven solutes in large-scale, statistically anisotropic media: Human health risk implications, *Water Resour. Res.*, *48*, W04527, doi:10.1029/2011WR011516.

## 1. Introduction

[2] Correctly identifying point values of a contaminant plume (i.e., at a well) is critical to accurately calculate human health risk because groundwater concentrations are often directly used as exposure values to assess risk. The importance of fundamental groundwater flow and transport processes in risk assessment has been demonstrated in multiple studies, but with varying methods. For example, risk assessments in which health risk is calculated with human exposure [e.g., *Andričević et al.*, 1994; *Hassan et al.*, 2001; *Tartakovsky*, 2007; *Bolster and Tartakovsky*, 2008], or conversely when human exposure is not calculated, and risk is defined as exceeding a threshold concentration such as a maximum contaminant level (MCL) or the risk of system failure [e.g., *Bolster et al.*, 2009; *Fernandez-Garcia et al.*, 2012]. Probabilistic approaches have also been used [e.g., *Andričević*, 1996; *de Barros and Rubin*, 2008], including a subset of probabilistic approaches which utilize a rigorous treatment of risk via uncertainty and variability methods [e.g., *Maxwell et al.*, 1999; *Smalley et al.*, 2000; *Benekos et al.*, 2007; *Maxwell et al.*, 2008; *de Barros et al.*, 2009; *Siirila et al.*, 2012]. *Maxwell and Kastenberg* [1999] found sorption mechanisms' influence on human health risk is small given intermediate and long exposure durations. Most recently, the influence of a contaminant's sorptive capacity was found to be a controlling factor in determining if risk exceeded United States Environmental Protection Agency (EPA) remediation action levels (RAL) [*Siirila et al.*, 2012]. Under an exposure duration of 30 years, differing degrees of instantaneous equilibrium sorption (referred to here as the local equilibrium assumption, LEA) yielded differing probabilities of an individual incurring cancer over a lifetime and/or experiencing an adverse health effect, where values of predicted risk varied by over an order of magnitude. Additionally, field and laboratory observations show nonideal or kinetic behavior of reactive solutes [e.g., *Pickens et al.*, 1981; *Roberts et al.*, 1986], suggesting the use of LEA in contaminant transport studies

[1]Hydrologic Science and Engineering Program, Colorado School of Mines, Golden, Colorado, USA.
[2]Department of Geology and Geological Engineering, Colorado School of Mines, Golden, Colorado, USA.
[3]Integrated Groundwater Modeling Center (IGWMC), Colorado School of Mines, Golden, Colorado, USA.


0043-1397/12/2011WR011516

may be problematic for accurately quantifying human health risk. This discrepancy and the finding of *Siirila et al.* [2012] which shows the importance of sorption mechanisms in assessing risk warrants further analysis of the assumption of LEA in risk assessment, and to identify the constraints of predictive tools to estimate when LEA is appropriate (for example, the Damköhler number as discussed in section 2.2.1).

[3] Deviations from LEA and the effects of kinetically sorbing solutes have been extensively studied in the past [*Jennings*, 1984; *Valocchi*, 1985; *Bahr and Rubin*, 1987; *Valocchi*, 1988; *Valocchi*, 1989; *Valocchi and Quinodoz*, 1989; *Cvetkovic and Shapiro*, 1990; *Andričević and Foufoula-Georgiou*, 1991; *Selroos and Cvetkovic*, 1992; *Dagan and Cvetkovic*, 1993; *Cvetkovic and Dagan*, 1994; *Selroos and Cvetkovic*, 1994; *Miralles-Wilhelm and Gelhar*, 1996; *Espinoza and Valocchi*, 1997; *Fiori and Bellin*, 1999; *Mishra et al.*, 1999; *Michalak and Kitanidis*, 2000; *Fiori et al.*, 2002] but not in the context of human health risk assessment. The majority of these studies derive or utilize analytical solutions that do not explicitly simulate well capture which is often necessary in predicting groundwater contamination and risk scenarios. Additionally, first-order analytical solutions are generally not valid at large variances of hydraulic conductivity, $K$ [m d$^{-1}$] [*Chin and Wang*, 1992; *Selroos and Cvetkovic*, 1992; *Selroos*, 1995; *Salandin and Fiorotto*, 1998]. While higher-order solutions exist, here we choose to use a numerical approach to allow for more flexibility in the level of problem complexity and the treatment of simplifying assumptions normally used in analytical solutions.

[4] The numerical framework utilized in this study is stochastic, where risk derived from groundwater well concentrations in three-dimensional heterogeneous media is assessed probabilistically. Specifically we investigate the effect of kinetically sorbing solutes in highly stratified aquifers, a topic addressed in the early literature for more simplified heterogeneous domains [*Valocchi*, 1988; *Valocchi*, 1989; *Cvetkovic and Shapiro*, 1990; *Andričević and Foufoula-Georgiou*, 1991]. Here we use stratified domains to assess realistic far-field groundwater contamination scenarios where variations in sedimentology and stratigraphy are dominant factors in determining contaminant flow and transport. Stratified aquifers are often associated with nonergodic transport [*Sánchez-Vila and Solís-Delfín*, 1999], or when the ensemble statistics do not coincide with the corresponding spatial averages calculated over a single realization [*Christakos*, 1992]. If the source dimensions are small with respect to the integral scale, highly stratified (i.e., highly anisotropic) aquifers have a higher uncertainty associated with the location of the plume center of mass and plume spreading. The stratified aquifer is also of interest because (1) the stratigraphy of many natural formations are highly anisotropic [see e.g., *Rubin*, 2003, Table 2.1] and (2) interconnected pathways are much more prevalent, where channeling of solutes through areas of higher hydraulic conductivity effectively decreases the overall effect of macrodispersion [*Siirila et al.*, 2012]. The importance of preferential flow paths was recently observed at the Macrodispersion Experiment (MADE) site, where highly asymmetric breakthrough curves suggest transport connectivity and where 43%–69% of particle paths are located within the high hydraulic conductivity zones [*Bianchi et al.*, 2011]. This study, however, only examines a small region of the aquifer (where domain size in $x$, $y$, and $z$ directions are $x_d = 4$, $y_d = 4$, $z_d = 6$ [m], respectively); it is one of the objectives of the current study to investigate how the effects of connectivity zones over short (i.e., meter scale) effect connectivity over larger distances (i.e., kilometer scale). This objective is achieved by up scaling aquifers of similar hydraulic composition (i.e., according to similar correlation lengths of [*Rehfeldt et al.*, 1992]) to the kilometer scale.

[5] In the present analysis, a case study (see section 3) is used to simulate an example contamination scenario involving mobilized arsenic, an aqueous contaminant that will sorb to mineral surfaces. Multiple ensembles (each composed of 200 realizations) of large extent, highly resolved, regional-scale aquifers are simulated with flow and transport codes through the use of parallel high-performance computing. Well elution breakthrough curves and time-dependent kinetic sorption are explicitly accounted for in this process. Because the methodology is numerical, high variances of $Y = \ln(K)$ [m d$^{-1}$] are also explored. Both the validity and predictability of LEA is investigated by stochastically simulating ensembles of both linear and kinetic sorption scenarios that should theoretically retard the solute equally if equilibrium is an appropriate assumption. An investigation of potential interplay (positive or negative feedbacks) between multiple hydrogeologic parameters is conducted for both kinetic and LEA ensembles. In particular, the effect of preferential flow pathways and solute mixing on the field-scale (marcrodispersion) and subgrid (local dispersion) is examined by a comparison of normalized well breakthrough curves and peak times for varying degrees of stratified, heterogeneous flow fields. Finally, carcinogenic human health risk is used as an endpoint of comparison by utilizing a risk methodology previously developed [*Maxwell and Kastenberg*, 1999; *Siirila et al.*, 2012]. Risk is calculated for a population of potentially exposed individual using a nested Monte Carlo approach, explicitly considering uncertainty in environmental parameters and variability in individual physiological and exposure parameters. These results have implications in a wide range of groundwater contamination scenarios involving reactive solutes, including but not limited to, acid-mine drainage, $CO_2$ leakage from Carbon Capture and Storage (CCS), other forms of underground waste storage, agricultural and urban runoff, disposal of industrial wastewater, etc.

## 2. Methodology

[6] Following the framework of *Siirila et al.* [2012], far-field groundwater flow and solute transport is modeled stochastically to account for uncertainty in groundwater flow paths. A complete set of the governing equations for (1) flow and transport, and for (2) human health risk are described in Appendices A and B, respectively. Section 2.1 briefly describes the creation of the heterogeneous aquifer, also consistent with the methodology previously presented by Siirila and coauthors. Section 2.2 outlines a number of new metrics used to analyze the interplay between reactive solutes and the hydrologic flow field. These metrics are useful tools to understand how modeling parameters affect

groundwater flow and transport and ultimately how they affect risk assessment analyses.

### 2.1. Hydrologic Flow Field and Heterogeneity

[7] Uncertainty in hydrologic flow and subsurface properties is accounted for by the use of a stochastic Monte Carlo scheme where multiple realizations of equally probable heterogeneous subsurface domains are simulated, all honoring the same global statistics. Although equally likely, each realization randomly simulates distinctly different hydraulic conductivity ($K$) [m d$^{-1}$] fields based on the geostatistical descriptors geometric mean ($K_g$) [m d$^{-1}$] and variance ($\sigma_Y^2$) [-] of $K$. An exponential correlation model is used to define spatial correlation of $K$ via a separation distance ($\xi$) [m] and correlation lengths in the horizontal and vertical directions ($\lambda_h$, $\lambda_v$, respectively) [m]:

$$R(\xi) = \sigma^2 \exp^{-\xi/\lambda_{h,v}}. \tag{1}$$

In this study, the magnitude of $\lambda_h$ is used to describe the degree of aquifer stratification and is a principal parameter investigated in the sensitivity analysis of the case study. The degree of stratification is discussed in terms of the statistical anisotropy ratio, $\varepsilon$ [-], equivalent to the ratio of vertical and horizontal correlation lengths ($\varepsilon = \lambda_v/\lambda_h$), and referred to hereafter as the anisotropy ratio. A very stratified formation is equivalent to $\varepsilon \ll 1$. This process yields realizations of flow dictated by the head gradient and spatially correlated random $K$ field which together comprise an ensemble of equally likely flow scenarios. By varying parameters such as $\varepsilon$ and the regional groundwater velocity ($v$ [m d$^{-1}$], see equation (A3)), multiple ensembles can be cross compared.

### 2.2. Transport of Sorbing Solutes

[8] Realizations of the flow field described in section 2.1 are linked to a solute transport model to simulate plume migration from a fixed source location. By linking flow field realizations with transport, ensembles of constant global statistics of flow *and* transport properties can be investigated. Sensitivity to these hydraulic properties is explored by generating multiple ensembles of varying hydraulic properties and analyzing the statistical outcome of an endpoint measured in the solute transport model (i.e., concentration at a well).

[9] Nonreactive (i.e., tracer), LEA, and first-order kinetic particle simulations are conducted. LEA simulations utilize the partition coefficient ($K_D$) [L kg$^{-1}$], defined as the slope of sorption isotherm relating the aqueous concentration in solution ($C$) [mg kg$^{-1}$] to the sorbed concentration in the solid phase ($C^*$) [mg m$^{-3}$]. Kinetic simulations utilize time-dependent forward ($k_f$) [L d$^{-1}$] and reverse ($k_r$) [kg d$^{-1}$] rates with an equivalent ratio to the partition coefficient:

$$K_D = \frac{k_f}{k_r} = \frac{C^*}{C}. \tag{2}$$

All sorption parameters ($K_D$, $k_f$, $k_r$) are constant in space and time. Here the retardation ($R$) [-] of the solute is directly related to $K_D$ for LEA simulations and the ratio ($k_f/k_r$) for kinetic simulations, where

$$R_{LEA} = 1 + \frac{\rho_b K_D}{\theta}, \tag{3}$$

$$R_{kin} = 1 + \frac{\rho_b k_f}{\theta k_r}, \tag{4}$$

where and $\theta$ [-] is porosity and $\rho_b$ [kg m$^{-3}$] is the bulk density of the porous medium. A stochastic element was added to the Lagrangian particle tracking model SLIM-FAST to rapidly and efficiently simulate the time dependence associated with kinetic sorption. This technique builds on previous approaches to decrease simulation time and improve computational efficiency [*Keller and Giddings*, 1960; *Valocchi and Quinodoz*, 1989; *Andričević and Foufoula-Georgiou*, 1991; *Tompson and Dougherty*, 1992; *Quinodoz and Valocchi*, 1993; *Michalak and Kitanidis*, 2000; *Maxwell et al.*, 2007]. When $k_f$ and $k_r$ rates are slow, reaction times are large and the particle displacements are small within a given advection time $t_{adv}$ [day], and result in long waiting times [e.g., *Valocchi and Quinodoz*, 1989]. Rather than explicitly simulating phase transfer between the porous media and solution, aqueous and sorbed times ($t_{aq}$ [day] and $t_s$ [day], respectively) during one $t_{adv}$ are monitored. $t_{aq}$ and $t_s$ are scaled by $k_f$ and $k_r$, in addition to a random number within a normal distribution ($RN$):

$$t_{aq} = \frac{RN}{k_f}, \tag{5}$$

$$t_s = \frac{RN}{k_r}. \tag{6}$$

When the sum of $t_{aq}$ and $t_s$ exceed the $t_{adv}$, $t_s$ is then added to the continuously running particle time ($t_{particle}$) [day]. This process is computed for each particle, $p$, for each advection step:

$$\begin{aligned} \text{Given} \quad & t_{aq,p} + t_{s,p} > t_{adv,p} \\ & t_p = t_p + t_{s,p} \end{aligned}. \tag{7}$$

In other words, the model is continuously moving particles according to the aqueous advection time (and therefore at a faster simulation rate) but accounts for kinetic sorption time by calculating a running tally of sorbed time. This process is especially efficient when forward and reverse rates are very fast in comparison to the groundwater velocity, effectively decreasing simulation time by several orders of magnitude over the approach previously used (see *Maxwell et al.* [2007] supplemental material for further particle tracking details). This approach is similar to the third of *Valocchi and Quinodoz*'s [1989] methods (the "Arbitrary Time step"), which was found to provide the most efficient method of simulating kinetic sorption with low simulation times, where the computational effort is quasi-independent of the reaction rate.

[10] Local (or subgrid) dispersion (LD) has also been linked to sensitivity in higher-order moments (i.e., mean solute point flux and concentration variances) [*Dagan and*

*Fiori*, 1997; *Fiori et al.*, 2002; *Fiorotto and Caroni*, 2002; *Bellin et al.*, 2004]. This increase in dispersion is quantified in terms of displacement by the nondimensional Péclet number (*Pe*) [-] and simplified through the relationship in equation (A6) as:

$$Pe = \frac{v_x \lambda_h}{D_L} = \frac{\lambda_h}{\alpha_L}. \quad (8)$$

LD has also been found to be especially significant in three-dimensional stratified aquifers, where given high *Pe* numbers and low $\varepsilon$, the neglect of LD may yield inaccurate results [*Bellin et al.*, 2004]. *Fiori* [1996] also had a similar finding for $\varepsilon \leq 0.1$, where both studies analyzed *Pe* numbers up to $O(10^3 - 10^4)$. Combinations of infinite ($Pe = \infty$) and finite ($Pe \neq \infty$) Péclet numbers of $O(10^4 - 10^5)$ at low anisotropy ratios ($\varepsilon \leq 0.1$) are simulated in this case study to examine aquifer settings where sedimentology and stratigraphy are controlling factors in flow and transport. Combinations of high *Pe* and low $\varepsilon$ have been briefly investigated in the literature [e.g., *Indelman and Dagan*, 1999] but not previously studied in risk assessment. Even if the aquifer is not highly stratified, *Fiorotto and Caroni* [2002] argue that it is important to include LD in the field of risk analysis where a threshold of safety is defined. A second stress on the investigation of LD in the case of stratified domain is made because other processes such as molecular diffusion and diffusive fractionation have been found to be controlling in nonequilibrium, or poorly mixed, regimes [*LaBolle et al.*, 2006]. Although the fundamental process and scales differ, *LaBolle et al.* [2006] found the importance of neighboring strata and hydrofacies (i.e., low and high-*K* zones) to be controlling in correctly dating post-1950, prebomb peak $^3$H and $^3$He water.

#### 2.2.1. LEA Prediction: The Damköhler Number

[11] The assumption that solutes instantaneously reach equilibrium is partly based on the postulation that groundwater velocities are slow relative to the rate of reaction, but is also widely used because of the reduction in complexity in the mass transport model [*Jennings*, 1984]. As noted earlier, this assumption may or may not be valid given certain hydrologic conditions. Traditionally, the use of the dimensionless Damköhler number has been used as a predictor to distinguish when LEA or kinetic modeling is appropriate [e.g., *Jennings*, 1984; *Bahr and Rubin*, 1987; *Brusseau and Srivastava*, 1997; *Espinoza and Valocchi*, 1997; *Michalak and Kitanidis*, 2000; *Green et al.*, 2010]. Although there are several definitions of the "length scale" used in the Damköhler definition, we choose to adapt the following, *local* formulation based upon the scale of the spatial discretization:

$$Da_{Local} = \frac{k_f * \Delta x}{\vec{v}} = \frac{k_f * \Delta x}{\sqrt{v_x^2 + v_y^2 + v_z^2}}, \quad (9)$$

where $\Delta x$ [m] is the cell size parallel to groundwater flow and $\vec{v}$ [m d$^{-1}$] is the cell based local velocity vector defined by directional components within that cell: $v_x$ [m d$^{-1}$], $v_y$ [m d$^{-1}$], $v_z$ [m d$^{-1}$]. It is important to note that because $k_f$ and $k_r$ rates are spatially homogeneous, any variance in *Da* is attributed to fluctuations in $\vec{v}$ (and therefore *Y*) alone. Likewise, we define a global estimate of the Damköhler number as:

$$Da_{Global} = \frac{k_f * \Delta x}{v}. \quad (10)$$

Following the aforementioned studies examining Damköhler numbers, large *Da* values, typically over 10.0 [-], suggest that the LEA is appropriate because the contaminant will have sufficient time to sorb to the porous media (i.e., sorption reaction time is small relative to the groundwater velocity). Likewise small *Da* values, typically below 1.0 [-], suggest that the contaminant will not have sufficient time to sorb to the porous media (i.e., sorption reaction time is large relative to the groundwater velocity) and may be treated as conservative. Intermediate *Da* values are rate limited, and forward and reverse kinetic modeling is needed. Theoretically, a Gaussian distribution of *Y* would yield a similarly Gaussian distribution of cell based velocities, and therefore a similar distribution of *Da* (Figure 1a). This is consistent with perturbation theory, where if according to equation (A1), ln(*K*) is described by $Y = <Y> + Y'$, *v* and *Da* may be described as $v = <v> + v'$ and $Da = <Da> + Da'$, respectively. This reasoning does not consider preferential flow pathways, or connected, high-*Y* zones where the velocity may be much faster than the predicted velocity given the statistical composition of the domain. Figures 1b, 1c, and 1d show an example cross section of the parametric relationship between *Y*, *v*, and *Da*. As expected, regions of high *Y* relate to regions of high *v* and regions of low *Y* relate to regions of low *v*. The *Y*-*v* relationship, however, is not completely linear due to the physical constraints of the flow regime. In contrast, the *v*-*Da* relationship is linear (see equations (9) and (10)). A comparison of Figures 1b and Figure 1d shows a clear *Y*-*Da* trend, where equilibrium zones (high *Da*) are associated with zones of low *Y*. To quantitatively investigate the impact of preferential flow pathways, one representative realization is used to calculate a distribution of *Da* for each flow field ensemble using the $Da_{Local}$ definition (equation (9)). A comparison to (equation (10)) is then conducted. Results of *Da* estimates and distributions are discussed in section 4.1.

#### 2.2.2. Analysis of Breakthrough Curves: Peak Concentration Distributions, Effective Retardations, Connectivity Indicator

[12] Four main parameters are adjusted in the following sensitivity analysis: $\varepsilon$, *v*, *Pe*, and the sorption scenario (i.e., LEA versus kinetic). To quantify the effects of each parameter adjusted, the flux averaged peak time ($t_{pk}$) [day] and normalized peak concentration ($C_{pk}/C_0$) [-] at which the maximum mass arrives at the well are calculated. $t_{pk}$ and $C_{pk}/C_0$ are computed for each well and each realization. Cumulative distribution functions (CDFs) shown here are composed of ($nw^*nr$) points, where *nw* is the number of wells within the domain, and *nr* is the number of realizations in the ensemble (i.e., 800 points per ensemble in this analysis). Ensemble CDFs are then compared (see section 4.2). CDFs of pulse and continuous sources are also examined given the same ensemble parameters. *Bellin and Rubin* [2004] found that peak concentration arrival time was a

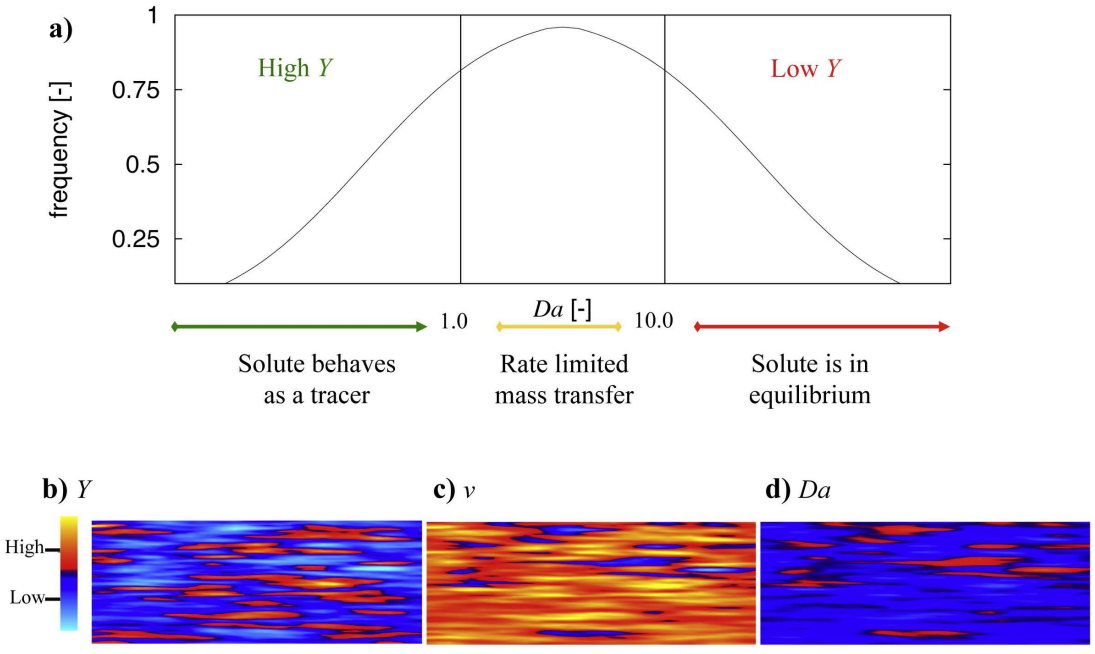


**Figure 1.** (a) Theoretical distribution of *Da* following a Gaussian distribution of *K*. (b–d) Identical cross sections showing the relationship between the variables (b) *Y*, (c) *v*, and (d) *Da*.

good proxy for advection dominated travel time. Peak arrival times are also of importance in the context of risk assessment, where the peak environmental concentration is averaged over an exposure duration (further details and discussion in Appendix B1).

[13] For each sorption scenario (LEA versus kinetic), effective retardation is expressed relative to $t_{pk}$ and $C_{pk}$ of the corresponding tracer simulation of that realization, where

$$R_{eff,LEA} = \frac{t_{pk,LEA}}{t_{pk,tracer}}, \tag{11}$$

$$R_{eff,kin} = \frac{t_{pk,Kin}}{t_{pk,tracer}}. \tag{12}$$

This essentially uses the conservative tracer simulations as a control by holding the parameters $\varepsilon$, $v$, and $Pe$, constant and isolating the effect of the sorption scenario alone. Equations (11) and (12) are based on the results of the numerical simulations and describe the effective retardation of the overall plume. $R_{eff,LEA}$ and $R_{eff,Kin}$ should not be confused with equations (3) and (4) which are used to calculate cell-based retardation within the model. Because of the relationship imposed between the ratio $k_f/k_r$ and $K_D$ (see equation (2)), if LEA is an appropriate assumption, $R_{eff,LEA}$ is equivalent to $R_{eff,Kin}$, regardless of the hydrologic domain or the transport parameters.

[14] To investigate the effect of LD, two metrics are used to calculate effective retardations. First, the differences between nonreactive breakthroughs are compared for $Pe = \infty$ and $Pe \neq \infty$ scenarios through the effective retardation of dispersion, $R_{eff,Disp}$

$$R_{eff,Disp} = \frac{[t_{pk,tracer}]_{Pe\neq\infty}}{[t_{pk,tracer}]_{Pe=\infty}}. \tag{13}$$

To isolate the effect of LD alone, equation (13) is calculated for the tracer simulations (i.e., excludes the sorption scenario). This metric holds the parameters $\varepsilon$, and $v$ constant while isolating the effect of $Pe$ alone.

[15] Because kinetic sorption is associated with tailing behavior [e.g., *Valocchi*, 1989], the additive effect of kinetics *and* dispersion is also investigated via the effective retardation of tailing, $\Delta R_{eff,Tail}$:

$$\Delta R_{eff,Tail} = [R_{eff,Kin}]_{Pe\neq\infty} - [R_{eff,LEA}]_{Pe\neq\infty}. \tag{14}$$

This metric holds the parameters $\varepsilon$ and $v$ constant and isolates the additive effect of tailing induced by LD *and* kinetic sorption. Theoretically this effective retardation resulting from $\varepsilon$ and $v$ can also be calculated, by following the same parameter isolation process. Because solute retardation scales linearly with $v$, the retardations of $\varepsilon$ and $v$ were not found to be controlling in this study and are therefore not presented in this work.

[16] Lastly, channeling through preferential flow paths is investigated by the connectivity indicator, *CI* [-]. As described by *Knudby and Carrera* [2005], the position of one point on the breakthrough curve (first-order moment) such as the peak or average concentration is proportional to the effective hydraulic conductivity, and does not relay information on flow connectivity. The shape of the breakthrough curve (higher-order moments), however, can be used to relate the degree of connectivity within an aquifer. Here we define *CI* as the ratio of the time at which 5% of particle mass is present at the well ($t_5$) [day], and the time at which 50% of the particle mass is present at the well ($t_{50}$) [day]:

$$CI = \frac{t_{50}}{t_5}. \tag{15}$$

A higher *CI* value signifies a breakthrough curve skewed toward earlier arrival times and significant tailing. Higher *CI* values indicate high channeling when compared to lower *CI* values [*Knudby and Carrera*, 2005]. Equation (15) was recently utilized in the work of *Bianchi et al.* [2011] and is based on the work of *Knudby and Carrera* [2005] but differs in that it does not utilize an area averaged exit face of the domain.

## 3. Description of Case Study

[17] A hypothetical contamination scenario of a potable drinking water aquifer is investigated in a fully saturated, regional-scale aquifer (approximately $x_d = 4000$ [m], $y_d = 1000$ [m], $z_d = 100$ [m]). 200 realizations of $Y$ and the subsequent hydrologic flow field were calculated by following the methodology described in section 2.1. Hydrologic parameters implemented ($K_g$, $\sigma_Y^2$, $\lambda_h/\lambda_v$) are typical of a fluvial or glacial outwash sand and gravel aquifer [*Springer*, 1991; *Rehfeldt et al.*, 1992; *Rubin*, 2003]. In this study two end member $\varepsilon$ are used to simulate aquifers with varying degrees of stratification. To allow for cross comparison of differing $\varepsilon$ ensembles, $\lambda_h$ is varied while $\lambda_v$ remains constant. Appropriate spatial sampling of the $Y$ field is implemented through a resolution of at least five cells per $\lambda_v$ and $\lambda_h$ [*Ababou et al.*, 1989], yielding a fine-scale discretization of $\Delta x = \Delta y = 3.0$ [m] and $\Delta z = 0.3$ [m] resulting in approximately 150 million compute cells. Due to the large number of cells per realization and the large number of realizations per ensemble, convergence below 1% was reached after 75 realizations in $\varepsilon = 0.1$ ensembles and below 0.1% in $\varepsilon = 0.006$ ensembles. Figure 2 shows representative realizations of each $\varepsilon$ ensemble. Additionally, three regional head gradients are simulated to produce varying degrees of $v$, spanning 3 orders of magnitude ($v = 0.001, 0.01, 0.1$ [m d$^{-1}$]). A hydraulic head gradient along the $x$ axis is imposed with constant head boundaries at the two faces of the domain parallel to the $y$ axis and enforcing

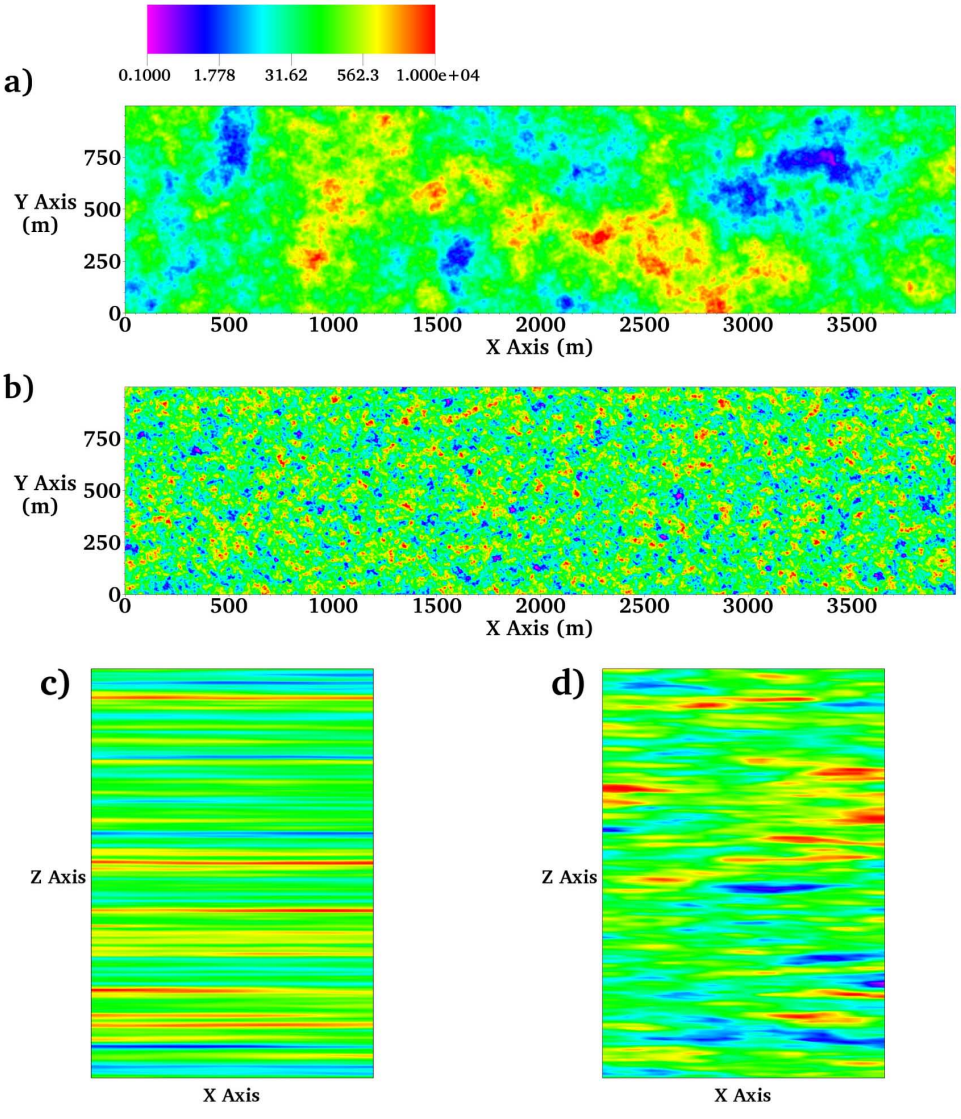


**Figure 2.** Representative realizations of $Y$ [m d$^{-1}$] fields for (a, c) a more stratified domain, $\varepsilon = 0.006$ [-], opposed to (b, d) a less stratified domain, $\varepsilon = 0.1$ [-]. Plan view is shown in Figures a and b and a segment of the vertical cross-sections is shown in Figures c and d.

no-flow boundaries at all other faces of the domain. Domains of each $\varepsilon$ are paired with each $v$, yielding six ensemble scenarios. These ensembles of varying hydraulic properties are used to simulate plume migration from a fixed source location up gradient of four groundwater pumping wells where contaminant mass is tracked as a function of time. Table 1 lists all flow parameters values used in the case study.

[18] Continuous and pulse sources of arsenic-contaminated groundwater are investigated, where the source concentration is assumed to be lognormally distributed based on the geochemical modeling of a source term in a previous study [*Siirila et al.*, 2012]. Arsenic is a worldwide contaminant of concern in groundwater resources and is furthermore of importance due to its high cancer and noncancer adverse health effects. Arsenic was also chosen for this case study due to its relatively mobile nature in comparison to other known toxins such as lead [*Siirila et al.*, 2012]. Human toxicity of arsenic has also been extensively studied in areas of naturally occurring, arsenic rich host rock material [*Nickson et al.*, 1998; *Berg et al.*, 2001; *Ogola et al.*, 2002; *Yu et al.*, 2003]. The US EPA ranks contaminants according to the amount of available data for a given contaminant from A (known human carcinogen) to E (evidence of noncarcinogenicity for humans). Arsenic is one of the few contaminants which is rated as "A", known human carcinogen, due to the vast number of studies which identify arsenic as the cause of cancers of the skin, lung, liver, and kidney [*Chen et al.*, 1992; *Guo et al.*, 1997]. One study estimated that at the previous US EPA maximum contaminant level (MCL) of arsenic (50.0 [ppb], now currently 10.0 [ppb]) at a water ingestion rate of 1.0 [L $d^{-1}$], as many as 13 out of every 1000 US persons are at risk of dying from liver, lung, kidney, or bladder cancers [*Smith et al.*, 1992]. As discussed in Appendix B, this probability greatly exceeds the US EPA remediation action levels, and stresses the need to accurately quantify US exposure to arsenic contamination. While the analysis here is based on the sorptive and toxicity values of arsenic, the results are generally applicable to a range of other contaminants with similar properties.

**Table 1.** Flow and Transport Parameter Values

| Parameter | Value | Units |
|---|---|---|
| Domain Size ($x_d$, $y_d$, $z_d$) | $\sim (4000 \times 1000 \times 100)$ | [m] |
| Cell discretization ($\Delta x$, $\Delta y$, $\Delta z$) | $(3.0 \times 3.0 \times 0.3)$ | [m] |
| Number of cells ($nx$, $ny$, $nz$) | $(1333 \times 333 \times 333)$ | – |
| Location of source ($x$, $y$, $z$) | (500.0, 500.0, 30.0) | [m] |
| Distribution of source $C$ | lognormal distribution | [$\mu$g $L^{-1}$] |
| Mean of source $C$ | 0.005 | [–] |
| Standard deviation of source $C$ | 0.55 | [–] |
| Number of particles | 300,000 | – |
| Geometric mean of $Y$ | $K_{G,Y} = 52$ | [m $d^{-1}$] |
| Standard deviation of $Y$ | $\sigma_Y = 1.9$ | – |
| Porosity | $\theta = 0.33$ | – |
| Well pumping rates | $Q_w = 500$ | [$m^3$ $d^{-1}$] |
| Well screen length | $s_w = 20$ | [m] |
| Well locations | $x_w = 3500, y_w = 800, z_w = 75;$ | [m] |
| | $x_w = 3500, y_w = 600, z_w = 75;$ | |
| | $x_w = 3500, y_w = 400, z_w = 75;$ | |
| | $x_w = 3500, y_w = 200, z_w = 75;$ | |
| *Anisotropy Ratios* | | |
| $\varepsilon = 0.1$ [-] | $\lambda_h = 15.0;$ | [m] |
| | $\lambda_v = 1.5$ | [m] |
| $\varepsilon = 0.006$ [-] | $\lambda_h = 250.0;$ | [m] |
| | $\lambda_v = 1.5$ | [m] |
| *Mean Groundwater Velocities* | | |
| $v = 0.001$ [m $d^{-1}$] | $\Delta h = 0.0317$ | [m] |
| $v = 0.01$ [m $d^{-1}$] | $\Delta h = 0.317$ | [m] |
| $v = 0.1$ [m $d^{-1}$] | $\Delta h = 3.170$ | [m] |
| *Sorption Scenarios* | | |
| LEA, partition coefficient | $K_D = 25$ | [L $kg^{-1}$] |
| *Kin1*, forward and reverse rates | $k_f = 2.88, k_r = 0.115$ | [L $d^{-1}$] |
| *Kin2*, forward and reverse rates | $k_f = 28.80, k_r = 1.150$ | [kg $d^{-1}$] |
| *Local Dispersion Scenarios* | | |
| $Pe = \infty$ [-] | $\alpha_L = 0.0, \alpha_T = 0.0$ | [m] |
| $Pe = 1.5 \times 10^4$ [-] | For $\lambda_h = 15.0;$ | |
| | $\alpha_L = 0.001, \alpha_T = 0.0001$ | [m] |
| $Pe = 2.5 \times 10^5$ [-] | For $\lambda_h = 250.0;$ | |
| | $\alpha_L = 0.001, \alpha_T = 0.0001$ | [m] |

[19] Solute transport of mobilized arsenic is modeled using the methodology described in section 2.2. For each of the six aforementioned flow field ensembles, plume migration is simulated utilizing LEA and first-order kinetic sorption. Two sets of kinetic forward and reverse rates are used (referred to hereafter as *Kin1* and *Kin2*) where the ratio of forward and reverse rates of each scenario are equivalent to each other and to the $K_D$ value used in the LEA simulations (see equation (2), $k_{f,Kin1}/k_{r,Kin1} = k_{f,Kin2}/k_{r,Kin2} = K_D$). Forward and reverse rates range by an order of magnitude, and are meant to be reflective of a range of literature values for arsenic [e.g., *Darland and Inskeep*, 1997; *Smith and Naidu*, 2009]. As described in section 2.2.2, if LEA is appropriate, the effective retardation of all sorption scenarios is equivalent ($R_{eff,LEA} = R_{eff,Kin1} = R_{eff,Kin2}$). The effect of LD is also investigated by simulating ensembles with ($Pe \neq \infty$) and without ($Pe = \infty$) this added parameter. Table 1 lists all transport parameter values used in the case study.

[20] For each ensemble, human health risk is calculated for the 99th fractile of variability (maximally exposed individual) following the methodology described in Appendix B. Risk to individuals within a population is calculated with exposure parameters based on the California, USA groundwater case study of *McKone and Bogen* [1991] and the references therein. Table 2 lists the generic exposure parameters used as suggested by the US EPA [*U.S.EPA*, 2001, 2004], as well as the arsenic toxicity values obtained and/or derived from the IRIS database. For each ensemble, 200 flow and transport realizations (uncertainty loop) were simulated and then resampled using a bootstrap method of 20,000 realizations to accurately characterize the source-term distribution. An additional 10,000 realizations of variability were then conducted for each uncertainty loop, resulting in 200 million Monte Carlo iterations per realization of the $K$ field.

## 4. Results and Discussion

### 4.1. Damköhler Number Distributions

[21] A global definition of the Damköhler number using equation (10) (see section 2.2.1) was used to estimate the extent to which LEA is valid for each case. Table 3 lists $Da_{Global}$ for varying $v$ and for both kinetic sorption rates. Using this predictor of solute behavior, equilibrium is expected for all scenarios, regardless of $k_f$ or $v$. To

**Table 2.** Exposure and Toxicity Parameter Values

| Parameter | Value | Units | Distribution[a] | Values | Source |
|---|---|---|---|---|---|
| Exposure duration | $ED$ | [year] | C | 30 | *US EPA RAGS* [2001] |
| Exposure frequency | $EF$ | [d yr$^{-1}$] | C | 365 | *US EPA RAGS* [2001] |
| Averaging time | $AT$ | [d] | C | 70 × 365 | *US EPA RAGS* [2001] |
| Ingestion rate per unit body weight | $IR/BW$ | [L kg d$^{-1}$] | L | ($3.3 \times 10^{-2}$, $1.3 \times 10^{-2}$) | *Mckone and Bogen* [1991] |
| Skin surface area per unit body weight | $SA/BW$ | [m$^2$ kg$^{-1}$] | L | ($2.7 \times 10^{-2}$, $2.5 \times 10^{-3}$) | *Mckone and Bogen* [1991] |
| Fraction of skin in contact with water | $f_{skin}$ | [-] | U | ($4.0 \times 10^{-1}$, $9.0 \times 10^{-1}$) | *Mckone and Bogen* [1991] |
| Shower exposure duration | $ED_{shower}$ | [h d$^{-1}$] | L | ($1.3 \times 10^{-1}$, $9.0 \times 10^{-2}$) | *Mckone and Bogen* [1991] |
| Unit conversion factor | $CF$ | [L m$^{-3}$] | C | $1.0 \times 10^{-3}$ | – |
| Cancer potency factor, ingestion | $CPF_{ing}$ | [kg d mg$^{-1}$] | C | 1.5 | IRIS |
| Cancer potency factor, dermal | $CPF_{derm}$ | [kg d mg$^{-1}$] | C | 1.58 | ($CPF_{ing}/ABS_{GI}$) |
| Gastrointestinal absorption | $ABS_{GI}$ | [-] | C | 95% | *US EPA RAGS* [2004] |
| Dermal permeability coefficient in water | $K_p$ | [m h$^{-1}$] | C | $1.0 \times 10^{-5}$ | *US EPA RAGS* [2004] |

[a]Constant (C) and lognormal (L) values represent the mean and standard deviation, respectively; Uniform (U) values represent the minimum and maximum values, respectively.

investigate to use of the Damköhler number as an indicator of macroequilibrium conditions, a distribution of $Da_{Local}$ numbers was also calculated for representative realizations of each of the six ensembles and for both kinetic rates using equation (9). Figure 3 shows the frequency of $Da_{Local}$ for varying $v$ (Figures 3a–3c) and $\varepsilon$ (see key of each part of Figure 3) in a single realization composed of $1.4 \times 10^8$ cells for both kinetic scenarios *Kin1* and *Kin2* (Figure 3 solid versus dashed lines, respectively). Regardless of $v$, $\varepsilon$, or $k_f$, a large distribution of $Da_{Local}$ is apparent, ranging from prediction of the solute akin to a tracer ($Da_{Local} \leq 1.0$), kinetically controlled ($1.0 \geq Da_{Local} \leq 10.0$), or in equilibrium ($Da_{Local} \geq 10.0$). A large frequency of $Da_{Local}$ values fall within nonequilibrium regimes, suggesting modeling with LEA may not be an appropriate assumption at all spatial locations within the domain. At this $\sigma_Y^2$, the distributions of $Da_{Local}$ for all scenarios are non-Gaussian, suggesting the relationship between $Y$ and $v$ (and therefore $Da_{Local}$) are nonlinear. This nonlinearity is expected due to the physical constraints on $v$, where $v$ is shown to vary more smoothly and has a smaller coefficient of variation in comparison to $Y$ [*Rubin*, 2003]. Here we see very little difference in $Da_{Local}$ distribution with changing $\varepsilon$, but a clear trend with increasing $v$. As $v$ increases, the tail of the $Da_{Local}$ distribution is smaller (i.e., reduced frequency of equilibrium cells) corresponding to a greater frequency of tracer and kinetic cells. The distributions of $Da_{Local}$ are also affected by the kinetic rate utilized, where the slower $k_f$ (*Kin1*) yields a distribution of $Da_{Local}$ skewed toward lower values and the faster $k_f$ (*Kin2*) yields a distribution of $Da_{Local}$ skewed toward higher values. This effect combined with the influence from varying $v$ suggests the slowest $v$ and the faster $k_f$ realization (Figure 3a, dashed lines) will contain the most cells in solute equilibrium. Likewise, the fastest $v$ and the slower $k_f$ realization (Figure 3c, solid lines) will contain the most cells out of equilibrium. The trends in $Da_{Local}$ (Figure 3) are comparable to the same trends in $Da_{Global}$ (Table 3), and are attributed to the linear dependence between $v$ and $k_f$ on $Da_{Local}$ and $Da_{Global}$.

**Table 3.** $Da_{Global}$ [-] Estimates

| | $v = 0.001$ | $v = 0.01$ | $v = 0.1$ |
|---|---|---|---|
| *Kin1* | 8640.0 | 864.0 | 86.4 |
| *Kin2* | 86,400.0 | 8640.0 | 864.0 |

While the results of $Da_{Local}$ expand on the first-order approximation using $Da_{Global}$, the distribution of local $Da_{Local}$ does not include path-dependent effects of the solute. Here we argue a more appropriate indicator of

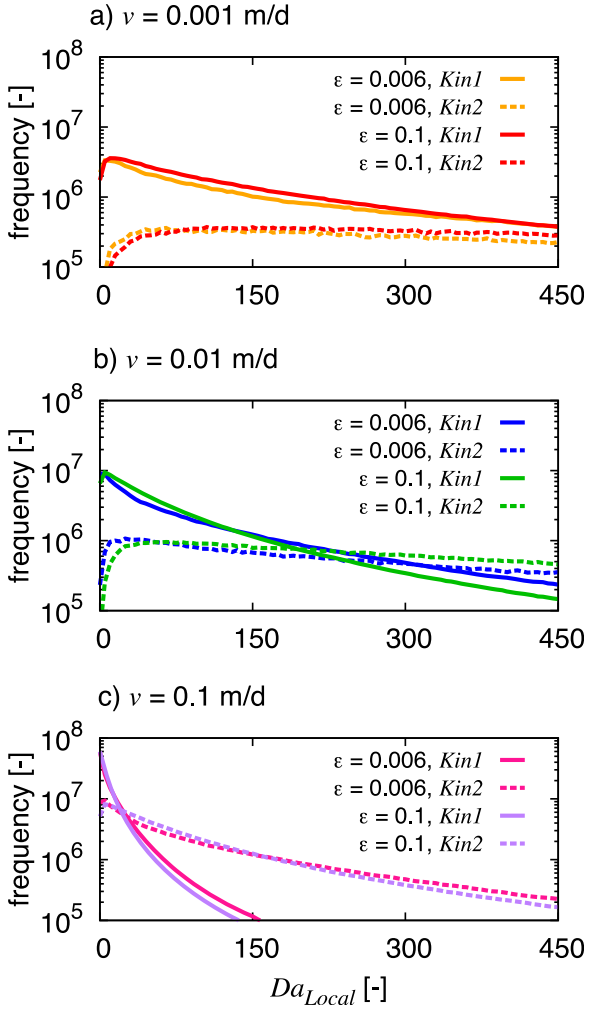


**Figure 3.** (a–c) Distributions of $Da_{Local}$ for the three varying mean groundwater velocities. Differences in anisotropy ratio are denoted by color; *Kin1* realizations are shown in solid lines whereas *Kin2* distributions are shown in dashed lines (see key of each subfigure).

equilibrium conditions is the *effective* retardation ($R_{eff}$) with respect to the *expected* retardation ($R$). General ensemble statistics are analyzed in sections 4.2–4.4 and calculated effective retardations are presented in section 4.3.

### 4.2. Peak Concentration Distributions

[22] The magnitude and distribution of the environmental concentration, independent of timing, are driving forces when assessing exposure (see Appendix B1). For each realization, and for each of the four wells, $C_{pk}/C_0$ is calculated using elution curves (see section 2.2.2). Figure 4 shows inner well ($y_w$ = 600 [m] and $y_w$ = 400 [m]) ensemble CDFs of $C_{pk}/C_0$ for a continuous source. The effects of varying $v$ (Figures 4a–4b, 4c–4d, 4e–4f), $\varepsilon$ (see key for each subplot), and $Pe$ (Figures 4a, 4c, 4e, and 4b, 4d, 4f) are compared. LEA distributions are shown as solid lines whereas *Kin1* distributions are shown in dashed lines. Results from *Kin2* distributions show great similarity to *Kin1* distributions and are therefore not presented here. The matrix of subplots shown in Figure 4 are used here to distinguish which combination of parameters (i.e., $v$, $\varepsilon$, $Pe$, and LEA versus *Kin1*) drive the magnitude and distribution variance of $C_{pk}/C_0$.

[23] Four general trends are noteworthy. Trend 1: an increase in $C_{pk}/C_0$ with an increase in $v$ (for example, the $x$ axis shift in Figures 4a and 4b compared to Figures 4e and 4f). This can be attributed an increase in effective recharge, where the regional head gradient increases in relation to the well pumping rate (which remains constant). In other words, if we define a dimensionless arrival time, $t_{arr,v} = Q_{regional,v}/Q_w$ (where $Q_{regional,v} = v^*\Delta z^* nz^* \Delta y^* ny$ is the regional volumetric flux, see Table 1 for further definitions), an increase in $C_{pk}/C_0$ increases linearly with $t_{arr,v}$. Trend 2: an increase in the $C_{pk}/C_0$ distribution variance with an increase in $v$ (for example, the smaller ensemble distribution in Figures 4a and 4b compared to Figures 4e and 4f) is attributed to an increase in macrodispersion within the aquifer, and thus more variability in the concentration at the well. Trend 3: an increase in the $C_{pk}/C_0$ distribution variance with a decrease in $\varepsilon$ (see the key in each subplot), is also attributed to an decrease in macrodispersion with $\varepsilon$. In the more stratified domain ($\varepsilon$ = 0.006), the aquifer is subject to lower solute spreading through channeling in interconnected $K$ zones. This channeling results in a binary distribution of the solute arriving at the well where elution water is either (1) clean, and the connected

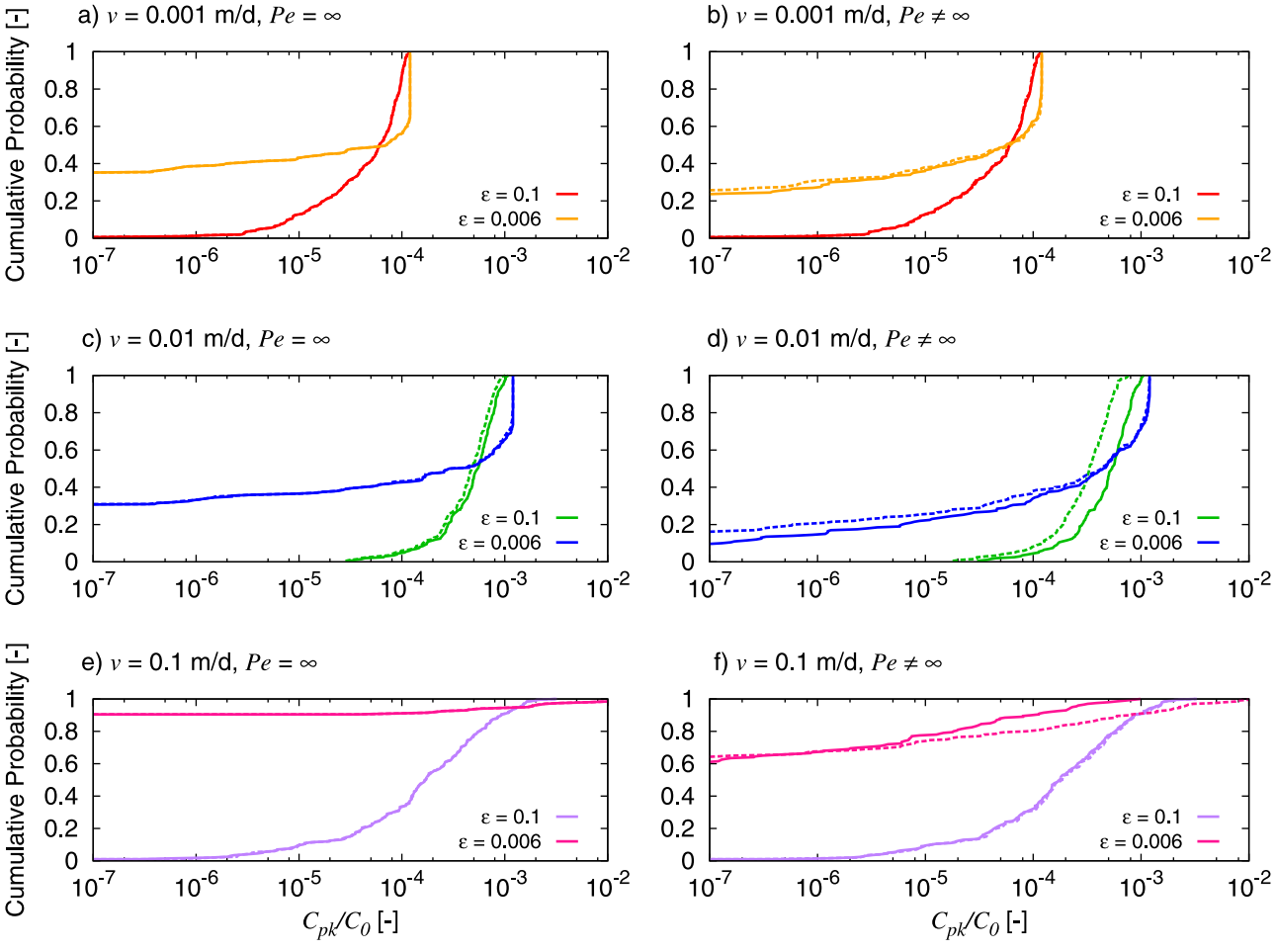


**Figure 4.** Cumulative distribution functions of $C_{pk}/C_0$ for varying $v$ (a–b, c–d, e–f) and $\varepsilon$ (see key for each subplot) using a continuous source. Infinite $Pe$ (a, c, e) and finite $Pe$ (b, d, f) are also shown. LEA distributions are shown in solid lines whereas *Kin1* distributions are shown in dashed lines.

zone does not follow a pathway connecting from the source to the well or (2) highly concentrated, and a connected zone between the source to the well exists. This behavior can be thought of as a "hit or miss" probability, increasing with $v$. This idea is consistent with that described by other previous studies, which show that in the absence of LD, the probability distribution function (pdf) model of point concentrations converge to a binary distribution [*Dagan*, 1982; *Sánchez-Vila and Solís-Delfín*, 1999; *Rubin*, 2003; *Bellin and Tonina*, 2007]. The latter references refer to studies involving tracers, where we note this behavior for reactive solutes. A quantitative discussion of results regarding channeling is presented in section 4.4.

[24] Trend 4: an increase in the $C_{pk}/C_0$ distribution variance with an increase in $Pe$ (see the smaller ensemble distributions in the left panel versus those in Figure 4, right) is related to the imposed LD within the model. While it is expected that the inclusion of LD will increase distribution variance, it should be noted that the cell-based mixing imposed for each cell is minute, equal to 1.0 [mm] in the longitudinal direction and 0.1 [mm] in the transverse direction (see Table 1). The increase in $C_{pk}/C_0$ distribution variance is physically relatable to the probability of pumping noncontaminated water from the well. For example, the percentage of clean groundwater withdrawal from a stratified aquifer varies between approximately 20%–90% whereas the less stratified aquifers are always pumping contaminated water. This result is in contrast to the molecular diffusion work of *Tartakovsky and Neuman* [2008], where an increase in $Pe$ yielded less mixing. In agreement with our results, *Tartakovsky and Neuman* [2008] also observed an increase in channeling with an increase in $Pe$. This study, however, only utilized a two dimensional domain and did not simulate spatial correlation of grain sizes. These limitations aside, this comparison suggests an up scaling of pore-scale diffusion to local dispersion may not be appropriate. These results also show agreement with those example simulations in the methodology presented by *Siirila et al.* [2012], which reported similar results for LEA distributions. Here we investigate the effect of time-dependent, kinetic sorption and the effect of time-dependent sorption in conjunction with LD (discussed in more detail below), in addition to how this metric ($C_{pk}/C_0$ CDF distributions) change with 3 orders of magnitude $v$, all topics which were not addressed in the methodology presented by *Siirila et al.* [2012]. This portion of the current discussion is the only overlying analysis with *Siirila et al.* [2012], shown here for completion and used as a discussion tool for other, new metrics in sections 4.3–4.5.

[25] To investigate if equilibrium is an appropriate assumption, CDFs of *Kin1* ensembles (dashed lines) are compared to CDFs of LEA ensembles (solid lines). For scenarios with $Pe = \infty$ (left panel of Figures 4a, 4c, and 4e) *Kin1* ensembles are nearly indistinguishable from LEA ensembles, suggesting LEA is an appropriate assumption for these hydro-geologic conditions. Unlike the $Pe = \infty$ ensembles, scenarios with $Pe \neq \infty$ (right panel of Figures 4b, 4d, and 4f) *Kin1* ensembles differ from LEA ensembles. In other words, with the inclusion of LD the equilibrium assumption is no longer valid given these hydro-geologic conditions. This is especially apparent for the more stratified domain ($\varepsilon = 0.006$), where for all $v$ the solute is out of equilibrium. The less stratified domain ($\varepsilon = 0.1$) is out of equilibrium for only the intermediate velocity (Figure 4d). The feedback between kinetic sorption and LD in stratified aquifers yielding disequilibrium conditions is an unexpected result, and highlights the complex interactions between time-dependent reactions are the hydro-geologic setting, as discussed in further detail below.

[26] Figure 5 shows the CDF results for a pulse source, and reflects the same formatting as Figure 4 for a continuous source. The magnitudes of $C_{pk}/C_0$ values are approximately 2 orders of magnitude lesser for ensemble CDFs of the pulse source (Figure 5) in comparison to the continuous source (Figure 4). The four general trends noted above for the continuous source are also true for the pulse source shown in Figure 5. *Kin1* ensembles (dashed lines) are clearly distinguishable from LEA ensembles (solid lines), suggesting LEA is not an appropriate assumption given these hydro-geological conditions. For all scenarios (Figures 5a–5f) LEA ensembles overestimate the magnitude of $C_{pk}/C_0$ values but do not dramatically affect the variance of the distribution. The lesser *Kin1* $C_{pk}/C_0$ values are attributed to delayed mass breakthrough at the well (i.e., a longer tailing effect). Thus, the effect of the time dependence in the pulse source (Figure 5) when compared to the time independent continuous source (Figure 4) is dominant in predicting equilibrium conditions. A disparity between $Pe \neq \infty$ (Figure 5, right) and for $Pe = \infty$ (Figure 5, left) is also apparent, where the inclusion of LD yields a more apparent difference between *Kin1* and LEA ensembles. This is attributed to the aforementioned additive effect between the time dependence in kinetic sorption and LD, also observed in ensembles utilizing the continuous source. These results show interdependence between kinetic sorption and LD not previously documented. Here the induced cell-based mixing creates particle jumps from interconnected high-$K$ regions into regions of low $K$ and vice versa.

[27] We speculate that the effect of the time dependence associated with kinetic sorption into and out of solution is magnified, yielding solute behavior unlike that of equilibrium simulations. This process is illustrated at the high-low-$K$ interface in the schematic representation shown in Figure 6 for LEA sorption (Figure 6a) and two possible kinetic sorption scenarios (Figures 6b and 6c). This schematic highlights the process of particle retardation when LD forces the particle into neighboring high or low $K$ zones. Particle movement at the time of LD ($t_{Disp}$, bottom panel of Figure 6) is indicated by particle locations 0–10, where equal time has elapsed between each incrementing particle location. Solid-end cap lines indicate the magnitude of particle displacement whereas vector lines indicate the magnitude of the groundwater velocity. The magnitude of particle velocity (or the velocity of the contaminant solute) is shown in the panel labeled $v_{particle}$. Because LEA is assumed in Figure 6a, the $v_{particle}$ is retarded by a factor of $R$ regardless of if the particle is located in a high- or low-$K$ zone (i.e., $v/R$, see equation (3) for definition of $R$). When kinetically controlled particles (Figures 6b and 6c), are located within a low-$K$ zone, $v_{particle}$ is analogously equivalent to $v/R$. The assumption here is that $v$ is much slower in low-$K$ zones than in high-$K$ zones, and is favorable to equilibrium conditions. This regime is akin to a high $Da$, and is illustrated by very similar particle displacements between

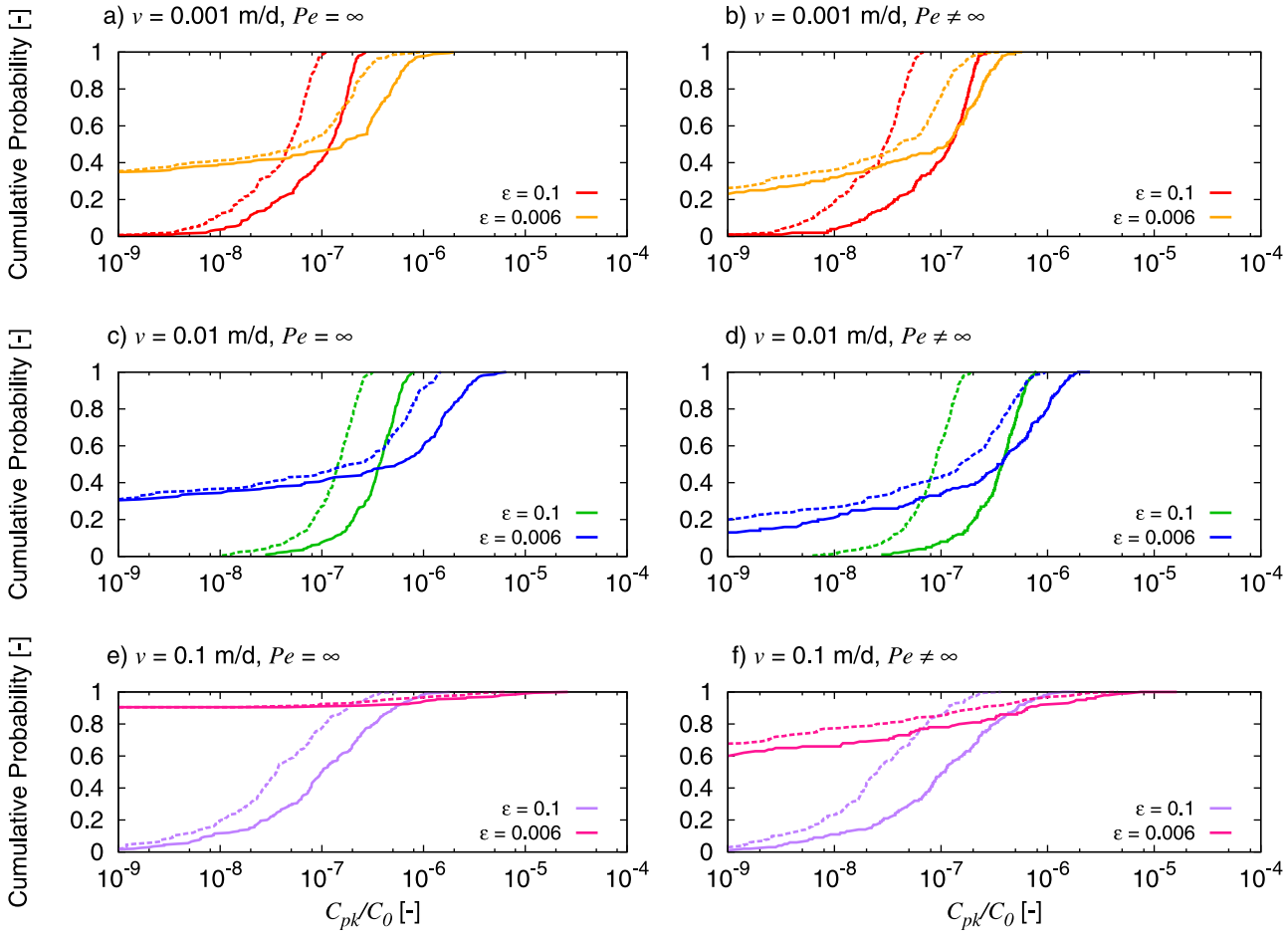


**Figure 5.** Cumulative distribution functions of $C_{pk}/C_0$ for varying $v$ (a–b, c–d, e–f) and $\varepsilon$ (see key for each subplot) using a pulse source term. LEA distributions are shown in solid lines whereas *Kin1* distributions are shown in dashed lines. Note the $x$-axis shown here is shifted two order of magnitude compared to that shown in Figure 4.

particle locations 1 and 2 for both LEA and kinetic scenarios. When kinetically controlled particles are located within a high-$K$ zone, $v_{particle}$ is equivalent to $v$ retarded by a factor of $R_{eff,kin}$ (i.e., $v/R_{eff,kin}$, see equation (4) for definition of $R_{eff,kin}$). Depending on the actual magnitude of $v$ in the high-$K$ zone, this regime is analogous to low and intermediate $Da$. An example of an intermediate (kinetic dependent) $Da$ is shown in Figure 6b, where $R_{eff,kin} < R$, and the particle displacement between particle locations 3 and 4 is larger in the kinetic case. The extreme case of very low $Da$ is depicted in Figure 6c, where the magnitude of $v$ in the high-$K$ zone is very high in relationship to the rate of the reaction, and $R_{eff,kin} \ll R$. As $R_{eff,kin}$ approaches unity, the particle is less retarded and behaves similar to a tracer. This is illustrated by the large particle displacement between locations 3 and 4. Our results, along with the conceptual model, indicate that there is an additive process involving kinetic sorption and LD that include: (1) particle retardation similar to LEA in low-$K$ zones where low $v$ regimes are conducive to equilibrium conditions, (2) lower particle retardation in high-$K$ zones via less reaction time in high-$v$ regimes, (3) shorter particle displacement in low-$K$ zones and longer particle displacements in high-$K$ zones, and (4) a higher frequency of $t_{Disp}$ in LEA scenarios compared to kinetic scenarios. A comparison of pulse and continuous sources show the kinetic-LD effect is greater for pulse sources, where time-dependent variables are more sensitive to this interaction. In addition to analyzing the magnitude and distribution of peak concentrations, section 4.3 discusses the results related to the timing of the sorbing solutes via effective retardation factors.

### 4.3. Effective Retardation Factor

[28] In addition to comparing normalized peak concentrations, corresponding peak times ($t_{pk}$) are also calculated. As discussed in section 2.2.2, $t_{pk}$ for each sorption scenario ($t_{pk,LEA}$ and $t_{pk,Kin1}$) are normalized by $t_{pk,tracer}$ (see equations (11) and (12)), effectively factoring out the effects of physical heterogeneity to analyze the sole effect of differences in *Kin1* and LEA ensembles. Figure 7 shows a scatterplot (12 ensembles, 200 realizations each) of effective kinetic retardations ($R_{eff,Kin1}$) versus normalized peak tracer concentrations ($C_{pk}/C_{pk,tracer}$) with infinite $Pe$ (Figures 7a, 7c, 7e) and finite $Pe$ (Figures 7b, 7d, 7f). To demonstrate the behavior of the majority of plume mass, only values corresponding to breakthrough mass greater than or equal to 5% of the source mass are shown. The crossbar intersection at $R_{eff} = 26$ [-] and $C_{pk,Kin1}/C_{pk,tracer} \approx 0.038$ [-]

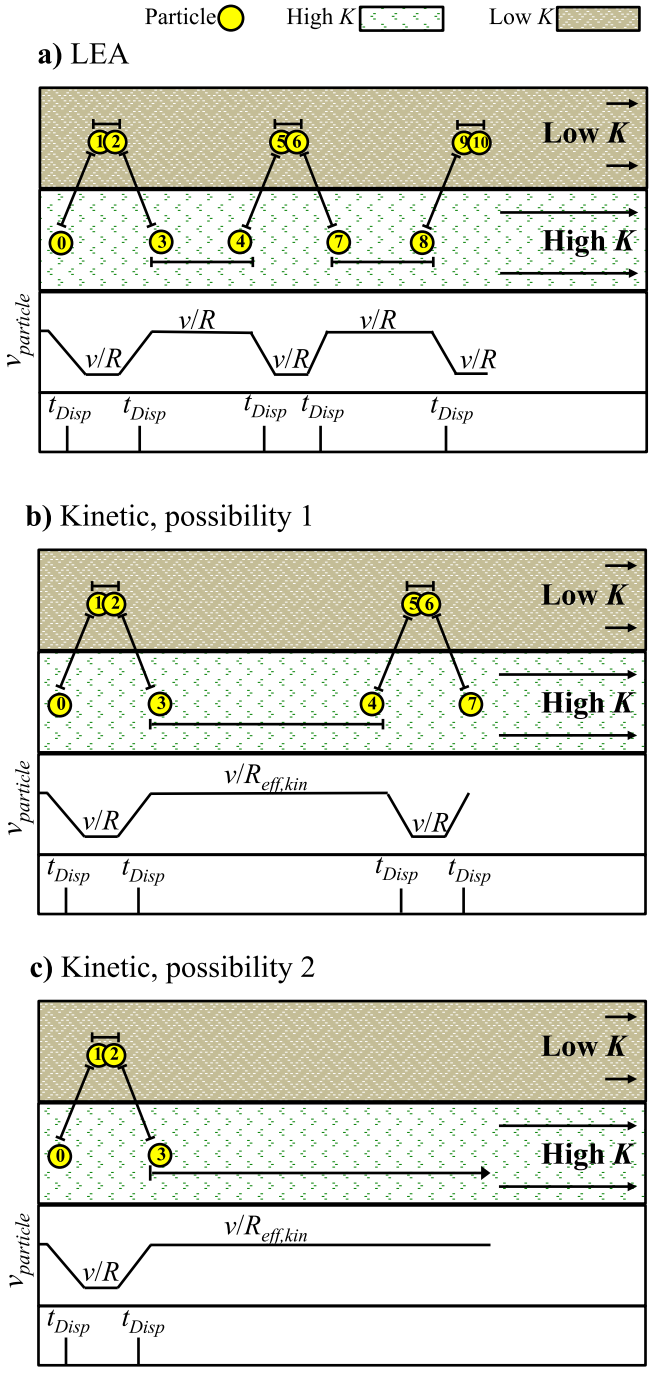


**Figure 6.** Schematic representation of the high-low-$K$ interface given LD for (a) LEA sorption and (b–c) two possible kinetic sorption scenarios.

corresponds to the expected solute retardation if equilibrium is an appropriate assumption. Results for *Kin1* simulations with a pulse source are shown here; LEA ensembles (not shown here) are centered at the crossbar intersection, as expected.

[29] As shown in Figures 7a–7f, *Kin1* ensembles are not centered at crossbar intersection but rather are centered between $R_{eff}$ = 40 – 70 [-] with corresponding $C_{pk,Kin1}/C_{pk,tracer}$ values less than 0.038. In other words, the majority of kinetic realizations yield a more retarded peak arrival time and concentration when compared to the LEA realizations, even though the expected retardations are equivalent. This result demonstrates the influence of the rate dependence associated with kinetic sorption, and how it potentially impacts both peak concentration and peak times. This behavior (i.e., the shift from expected intercept in Figure 7) is evident across 3 orders of magnitude of $v$, including the $v = 0.001$ [m d$^{-1}$] cases that have the highest potential of the three $v$ for equilibrium conditions to persist. This result furthermore demonstrates the impact of kinetic sorption in these simulations and in other potential hydrologic conditions.

[30] Second, while the majority of the scatter is shifted toward greater $R_{eff}$ values (i.e., more retarded peak times), several realizations show much smaller $R_{eff}$ values, and therefore very fast arrival times. This is especially true for finite *Pe* ensembles (Figure 7, right). The faster peak times can again be explained by the schematic in Figure 6, where the increase in LD in kinetic simulations may move a particle from a region of low to high $K$, increasing the probability of aquifer channeling. This result with respect to time is consistent with the results with respect to concentration as discussed in section 4.2, where the centered value of $R_{eff}$ for finite *Pe*, *Kin1* ensembles is nearly double that of LEA ensembles. Differences in stratification are also apparent in Figure 7, where smaller $\varepsilon$ demonstrate less variance in $R_{eff}$ and greater $\varepsilon$ demonstrate more variance in $R_{eff}$. In other words, the normalized arrival times for more stratified domains are consistent in contrast to the less consistent arrival times with the less stratified domain. This effect can also be attributed to channeling and preferential flow pathways in the stratified domain.

[31] The effective retardation of dispersion, $R_{eff,Disp}$, is used to isolate the effect of LD through the use of equation (13). As outlined in section 4.2, this metric is performed on tracer simulations only in order to separate the effect of the sorption scenario. Figure 8 shows $R_{eff,Disp}$ versus $[C_{pk}]_{Pe\neq\infty}/[C_{pk}]_{Pe=\infty}$ at both $\varepsilon$ (see subplots) for varying $v$ (Figures 8a–8c). Summary statistics are also shown in Table 4. Regardless of $v$, the driver in $R_{eff,Disp}$ behavior is the difference in $\varepsilon$. The less stratified domain ($\varepsilon = 0.1$) exhibits little difference between finite and infinite *Pe*, as shown by a clustered $R_{eff,Disp}$ near unity ($R_{eff,Disp} = 1$, $C_{pk}/C_0 = 1$). In contrast, the stratified domain ($\varepsilon = 0.006$) exhibits scatter far from the unity point. A majority of this scatter (>50% of points) falls within quadrants II and IV in Figures 8a–8c. Quadrant II reflects when:

[32] 1. $(t_{pk,Pe\neq\infty}) \leq (t_{pk,Pe=\infty})$,

[33] 2. $(C_{pk,Pe\neq\infty}) \geq (C_{pk,Pe=\infty})$.

[34] In other words, when the inclusion of LD yields a faster peak time and a higher concentration. Quadrant IV reflects when:

[35] 1. $(t_{pk,Pe\neq\infty}) \geq (t_{pk,Pe=\infty})$,

[36] 2. $(C_{pk,Pe\neq\infty}) \leq (C_{pk,Pe=\infty})$.

[37] Or, when the inclusion of LD yields a slower peak time and a lower concentration. The $\varepsilon = 0.006$ scatter in quadrant II reflects when the inclusion of LD forces the contaminant from zones of low $K$ into zones of higher $K$. Similarly, $\varepsilon = 0.006$ scatter in quadrant IV reflects movement from zones of high $K$ into zones of lower $K$. This finding suggests the inclusion of LD (even if only on the mm scale) will cause either a retardation or acceleration of the

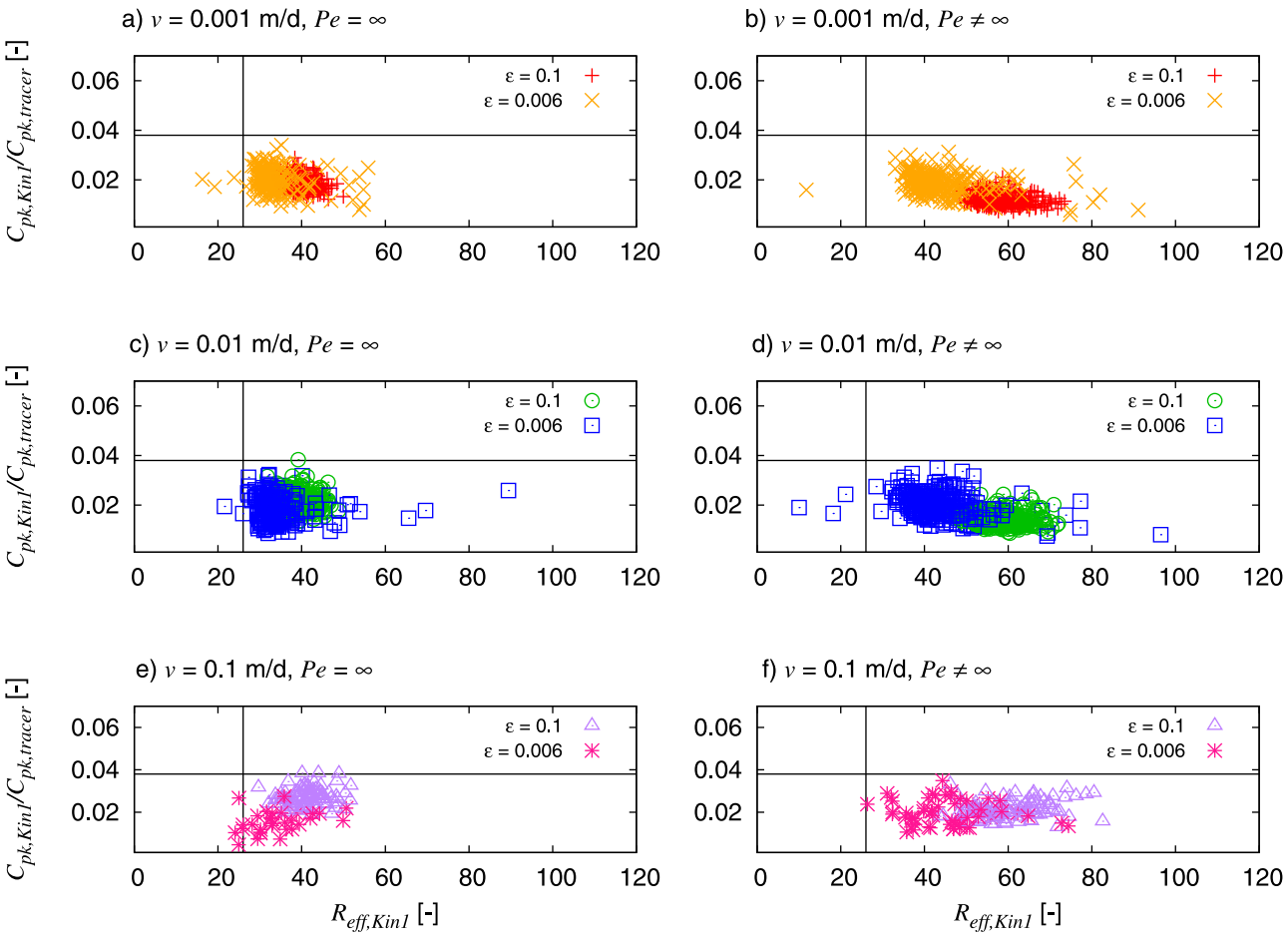


**Figure 7.** *Kin1* effective retardation ratios versus normalized peak concentrations for each realization of the six instantaneous pulse-source ensembles for (a, c, e) infinite *Pe* and (b, d, f) finite *Pe*. Differences in $v$ and $\varepsilon$ are denoted by color and symbol (see key for each subplot).

overall plume. While other studies have shown the effect of LD affects higher-order moments [*Dagan and Fiori*, 1997; *Fiori et al.*, 2002; *Fiorotto and Caroni*, 2002; *Bellin et al.*, 2004], to the best knowledge of the authors, the theory of LD as a catalyst of retardation of the first-order moment has yet to be reported (represented here as the peak time and concentration). This result regarding LD builds on the previous theories regarding diffusion suggested by LaBolle and coauthors [*LaBolle et al.*, 2006; *LaBolle et al.*, 2008]. The effect of kinetic sorption is isolated from this result, and is therefore applicable (and has implications) in the theory of nonsorbing solutes as well.

[38] The last effective retardation calculated is also discussed in section 2.2.2 and reflects the additive effect of tailing induced by LD and kinetic sorption, referred to here as $\Delta R_{eff,Tail}$. Equation (14) is used to calculate this additive effect, and is tabulated in Table 4. These statistics quantitatively measure the differences in effective retardation between LEA ensembles without LD (not plotted here, but centered around $R_{eff,LEA} = 26$ [-]) and *Kin1* ensembles with LD (right panel of Figure 7). The average $\Delta R_{eff,Tail}$ (see Table 4, $\overline{\Delta R_{eff,Tail}}$) is considerably larger for the less stratified domain ($\varepsilon = 0.1$) than for the stratified domain ($\varepsilon = 0.006$). The standard deviation of $\Delta R_{eff,Tail}$ (see Table 4, $\sigma_{\Delta R_{eff,Tail}}$) is larger for the less stratified domain when compared to the stratified domain. These results suggest the additive effect from kinetic sorption and LD affect the effective retardation of both stratification scenarios, but in different ways. The $\overline{\Delta R_{eff,Tail}}$ for $\varepsilon = 0.1$ ensembles is more consistently affected by the tailing effect when compared to the $\varepsilon = 0.006$ ensembles. Because the $\sigma_{\Delta R_{eff,Tail}}$ of the $\varepsilon = 0.006$ ensembles is large (8.3 – 11.6 for all $v$) when compared to $\varepsilon = 0.1$ ensembles (4.7 – 8.4 for all $v$), the additive tailing effect is also pronounced, but not as consistently. Table 4 also shows $\sigma_{\Delta R_{eff,Tail}}$ increases with greater $v$, an artifact of increased plume spreading with increased $v$. Interestingly, the relationship between $\overline{\Delta R_{eff,Tail}}$ and $v$ is unclear, where the intermediate $v$ does not correspond to intermediate $\overline{\Delta R_{eff,Tail}}$ values but rather minimum $\overline{\Delta R_{eff,Tail}}$ values. This analysis of $\Delta R_{eff,Tail}$ demonstrates the pronounced solute tailing effect that would otherwise be neglected if the two modeling assumption (LEA and $Pe = \infty$) were presumed. These small-scale differences in transport and how they affect both concentration and human health risk are further discussed in section 4.4.

### 4.4. Measure of Aquifer Channeling

[39] To investigate aquifer connectivity, the connectivity indicator (*CI*) metric is utilized in conjunction with

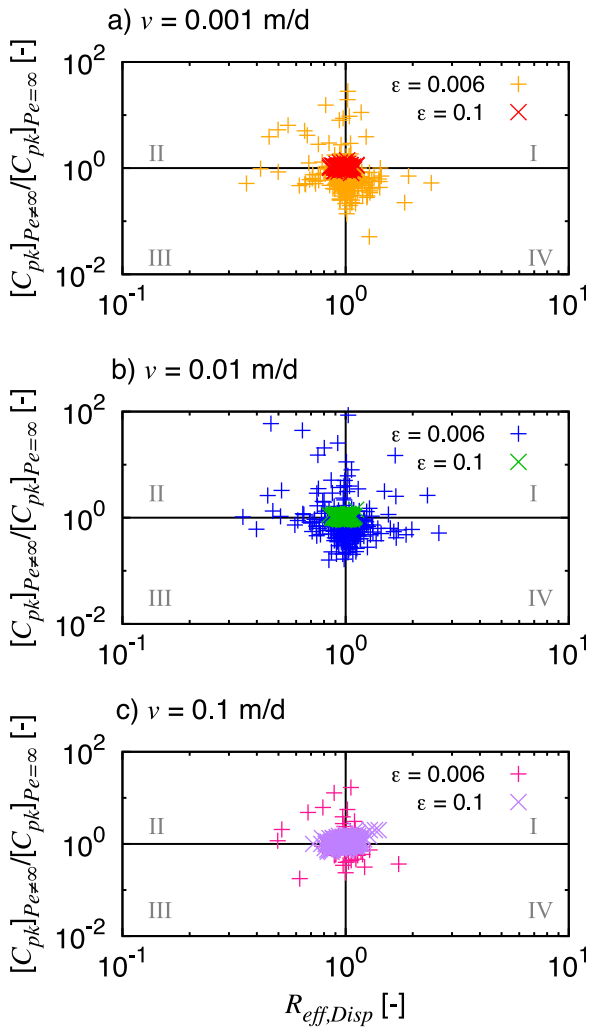


**Figure 8.** Effective retardation of dispersion versus normalized peak concentration for varying $v$ (a–c) and $\varepsilon$ (see key for each subplot). Ensembles reflect a pulse source only.

breakthrough times corresponding to when 50% and 5% of the mass arrives at the well (see equation (15)). Table 5 shows statistics corresponding to the average connectivity indicator ($\overline{CI}$) [-] and standard deviation of the connectivity indicator ($\sigma_{CI}$) [-] for varying $v$, $Pe$, and sorption scenarios.

[40] General trends in $\overline{CI}$ include: (1) greater $\overline{CI}$ for kinetic sorption ensembles and lesser $\overline{CI}$ for LEA ensembles, (2) greater than or equal $\overline{CI}$ in ensembles including LD and lesser or equal $\overline{CI}$ ensembles excluding LD. This analysis also indicates $\overline{CI}$ is invariant to differences in $\varepsilon$. The higher $CI$ values within Table 5 signify a breakthrough curve

**Table 5.** *CI* Statistics[a]

| | $v = 0.001$ | | $v = 0.01$ | | $v = 0.1$ | |
|---|---|---|---|---|---|---|
| | $CI$ | $\sigma_{CI}$ | $CI$ | $\sigma_{CI}$ | $CI$ | $\sigma_{CI}$ |
| | | | $\varepsilon = 0.1$ | | | |
| LEA | | | | | | |
| $Pe = \infty$ | 1.31 | 0.03 | 1.31 | 0.03 | 1.31 | 0.03 |
| $Pe = 1.5 \times 10^4$ | 1.31 | 0.03 | 1.31 | 0.03 | 1.30 | 0.02 |
| *Kin1* | | | | | | |
| $Pe = \infty$ | 1.53 | 0.05 | 1.49 | 0.03 | 1.64 | 0.05 |
| $Pe = 1.5 \times 10^4$ | 1.64 | 0.06 | 1.46 | 0.04 | 1.70 | 0.08 |
| *Kin2* | | | | | | |
| $Pe = \infty$ | 1.53 | 0.05 | 1.47 | 0.04 | 1.53 | 0.06 |
| $Pe = 1.5 \times 10^4$ | 1.64 | 0.06 | 1.46 | 0.04 | 1.66 | 0.09 |
| | | | $\varepsilon = 0.006$ | | | |
| LEA | | | | | | |
| $Pe = \infty$ | 1.33 | 0.25 | 1.35 | 0.30 | 1.33 | 0.19 |
| $Pe = 2.5 \times 10^5$ | 1.50 | 0.25 | 1.49 | 0.26 | 1.45 | 0.17 |
| *Kin1* | | | | | | |
| $Pe = \infty$ | 1.48 | 0.32 | 1.50 | 0.26 | 1.72 | 0.19 |
| $Pe = 2.5 \times 10^5$ | 1.65 | 0.34 | 1.61 | 0.22 | 1.79 | 0.21 |
| *Kin2* | | | | | | |
| $Pe = \infty$ | 1.48 | 0.32 | 1.45 | 0.28 | 1.46 | 0.18 |
| $Pe = 2.5 \times 10^5$ | 1.65 | 0.34 | 1.59 | 0.23 | 1.60 | 0.23 |

[a]Ensembles reflect a pulse source only.

skewed toward earlier arrival times and significant tailing. These results are consistent with the analysis presented in section 4.3, where it was shown that the resulting solute peak concentration from kinetic sorption and/or LD is retarded in time. General trends in $\sigma_{CI}$ provide a more insightful discussion, and include: (1) greater $\sigma_{CI}$ for kinetic sorption ensembles and lesser $\sigma_{CI}$ for LEA ensembles, (2) much greater $\sigma_{CI}$ in stratified aquifers ($\varepsilon = 0.006$) in comparison to the less stratified aquifers ($\varepsilon = 0.1$). $\sigma_{CI}$ is invariant to differences in LD. Trend 2 is the most pronounced result, suggesting connectivity is highly variable within the $\varepsilon = 0.006$ ensembles and not within the $\varepsilon = 0.1$ ensembles. $CI$ values within highly stratified aquifers are as high as 3.9 [-], and as low as 1.0 [-] where multiple realizations of the ensemble are dominated by either very fast or slow flow paths. Very high $CI$ values are indicative of fast paths from the source to the well, and vice versa for very low $CI$ values. This behavior signifies $\sigma_{CI}$ is a better metric for connectivity in comparison to $\overline{CI}$. $v = 0.001$ [m d$^{-1}$], $\varepsilon = 0.006$ ensembles at both sorption rates (*Kin1* and *Kin2*) yield the highest $\sigma_{CI}$ values, indicating kinetic sorption is controlling in the shape of the breakthrough curve. Finite $Pe$ of these ensembles ($\varepsilon = 0.006$, *Kin1* and *Kin2*) compared to infinite $Pe$ also contributes to greater $\sigma_{CI}$, supporting the aforementioned finding concerning a positive feedback between kinetic sorption and LD. We postulate a greater $\sigma_{CI}$ in the case of kinetically driven, stratified domains is again physically explainable by the schematic

**Table 4.** Change in Effective Retardation of Dispersion and Effective Retardation of Tailing Statistics[a]

| | $v = 0.001$ | | | | $v = 0.01$ | | | | $v = 0.1$ | | | |
|---|---|---|---|---|---|---|---|---|---|---|---|---|
| | $\overline{R_{eff,Disp}}$ | $\sigma_{Reff,Disp}$ | $\overline{\Delta R_{eff,Tail}}$ | $\sigma_{\Delta Reff,Tail}$ | $\overline{R_{eff,Disp}}$ | $\sigma_{Reff,Disp}$ | $\overline{\Delta R_{eff,Tail}}$ | $\sigma_{\Delta Reff,Tail}$ | $\overline{R_{eff,Disp}}$ | $\sigma_{Reff,Disp}$ | $\overline{\Delta R_{eff,Tail}}$ | $\sigma_{\Delta Reff,Tail}$ |
| $\varepsilon = 0.1$ | 1.03 | 0.05 | 32.48 | 4.70 | 1.03 | 1.85 | 31.46 | 5.05 | 1.09 | 1.91 | 34.81 | 8.41 |
| $\varepsilon = 0.006$ | 1.15 | 2.62 | 18.65 | 8.50 | 0.04 | 7.08 | 17.74 | 8.29 | 0.18 | 3.09 | 19.71 | 11.56 |

[a]Ensembles reflect a pulse source only.

shown in Figure 6, where LD may induces particles originally located in low-$K$ zones into high-$K$ channels and yield a lower effective retardation of the particle (or vice versa), thus increasing the distribution of $\sigma_{CI}$.

### 4.5. Carcinogenic Risk

[41] The probability of an individual incurring carcinogenic cancer risk was calculated using the framework in the work of *Siirila et al.* [2011] and equations presented in Appendix B, sections B1–B3. Uncertainty and variability was considered following the nested Monte Carlo scheme presented in section B4. Figure 9 shows cancer risk given a continuous source for infinite *Pe* (Figure 9a) and finite *Pe* (Figure 9b). Figure 10 shows cancer risk given a pulse source for infinite *Pe* (Figure 10a) and finite *Pe* (Figure 10b). Both Figures 9 and 10 show cancer risk to the maximally exposed individual (99th fractile of variability) at the 5th, 50th and 95th percentile of uncertainty (shown here as upper and lower bound around the 50th percentile of uncertainty). Varying $v$ ($x$ axis) is presented for differences in $\varepsilon$ for the six flow field ensembles (see color key shown in Figure 8). LEA distributions are shown in solid lines whereas *Kin1* distributions are shown in dashed lines, yielding 12 ensembles of risk per *Pe* scenario and 24 ensembles of risk per source scenario. Remediation action and *de minimus* levels are also plotted as horizontal lines at $10^{-6}$ [-] and $10^{-4}$ [-]. The following is a discussion of a comparison between these 24 ensembles and implications of the disparities between them.

#### 4.5.1. Continuous Source Risk

[42] Figure 9a shows the probability of risk given a continuous source term and infinite *Pe*. As $v$ increases, the upper bound (95th percentile) of risk also increases. Differences in $\varepsilon$ are small for the $v = 0.001$ [m d$^{-1}$] and $v = 0.01$ [m d$^{-1}$], but drastically affect the distribution of risk at the fastest $v$, where the more stratified domain ($\varepsilon = 0.006$, pink lines) has an upper bound cancer risk higher than the $10^{-4}$ remediation action level and a mean cancer risk much lower than the *de minimis* remediation action level (less than $10^{-10}$ [-]). In other words, the scientific uncertainty associated with the risk of cancer from a stratified domain with high $v$ is substantial (i.e., highly uncertain) but also relates to the highest cancer risk of all flow field scenarios. As explained with the *CI* metric (Table 5), stratified domains have a much higher associated variance in connected pathways (i.e., very fast or very slow fingering). The elution concentration at the well is therefore very low (near or equal to zero) or very high (unmixed, highly concentrated solutes). As shown here, the dependence on groundwater flow

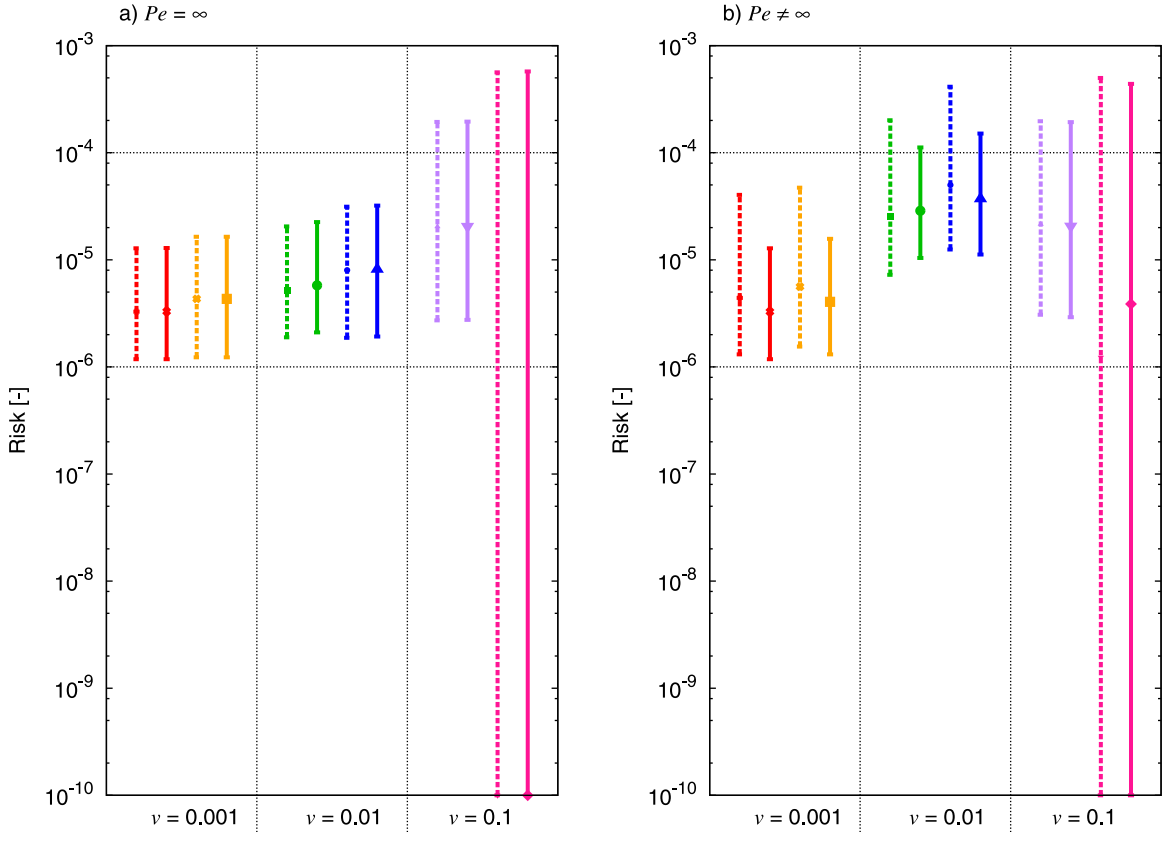


**Figure 9.** Increased cancer risk for the maximally exposed individual (99th fractile of variability) for a continuous source term is shown for (a) infinite *Pe* and (b) finite *Pe*. The 99th and 5th percentiles of uncertainty are plotted as upper and lower bounds around the mean (50th percentile) for each ensemble. Varying $v$ is also shown ($x$-axis) for differences in $\varepsilon$ (see color key shown in Figure 8). LEA distributions are shown in solid lines whereas *Kin1* distributions are shown in dashed lines.

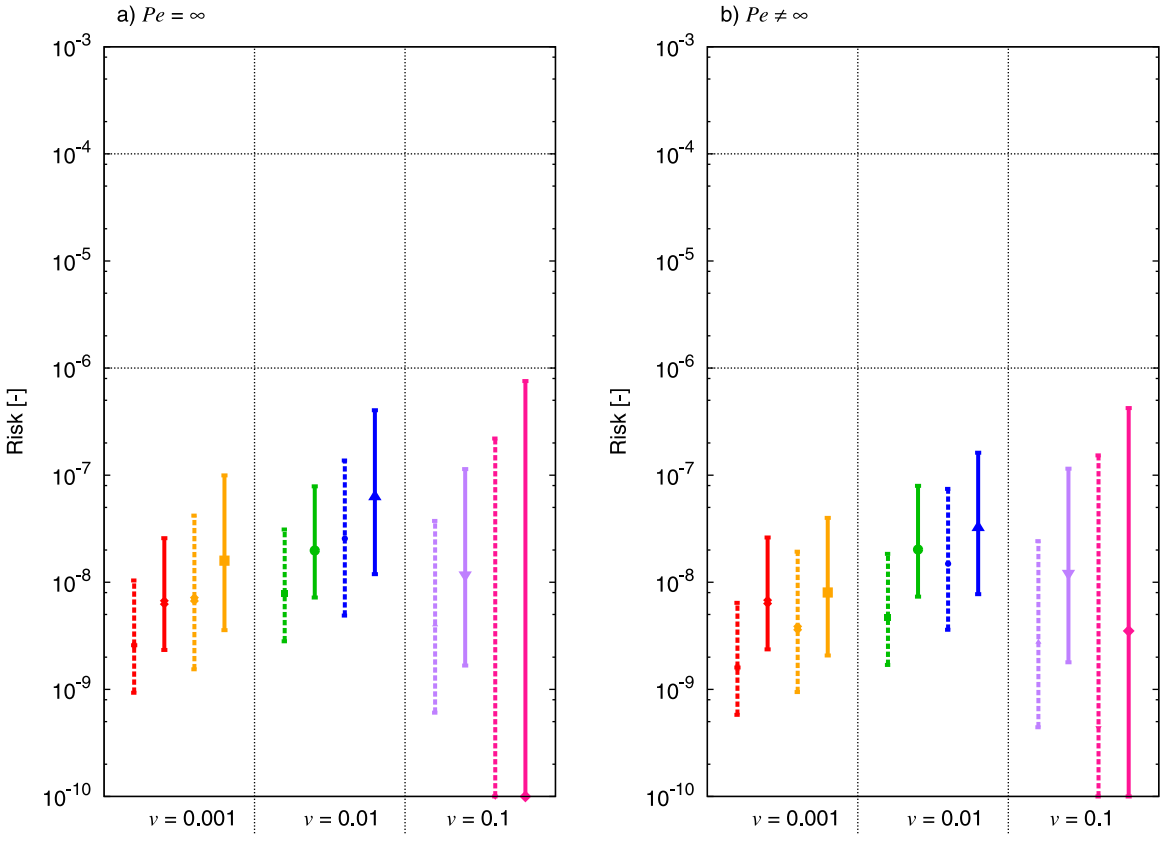


**Figure 10.** Increased cancer risk for the maximally exposed individual (99th fractile of variability) for a pulse source term is shown for (a) infinite *Pe* and (b) finite *Pe*. The 99th and 5th percentiles of uncertainty are plotted as upper and lower bounds around the mean (50th percentile) for each ensemble. Varying $v$ is also shown ($x$-axis) for differences in $\varepsilon$ (see color key shown in Figure 8). LEA distributions are shown in solid lines whereas *Kin1* distributions are shown in dashed lines.

pathways are directly related to the distribution and magnitude of risk estimates. Differences in the sorption scenario (Figure 9a, dashed versus solid lines) are indistinguishable, consistent with the results found in Figures 4a, 4c, and 4e. For these 12 ensembles (continuous source, infinite *Pe*), LEA is a correct assumption, and was accurately predicted by $Da_{Global}$.

[43] Figure 9b shows the probability of risk given a continuous source term and finite *Pe*. In general, as $v$ increases, the risk upper bound (95th percentile of uncertainty) also increases. An exception exists for the less stratified, fastest $v$ ensembles (Figure 9b, purple lines) and is discussed below. Variations in $\varepsilon$ also show dependence in trends with $v$. Changes in risk with changes in $\varepsilon$ are small for $v = 0.001$ [m d$^{-1}$] (red versus orange lines) and are more distinct for $v = 0.01$ [m d$^{-1}$] and $v = 0.1$ [m d$^{-1}$] (green versus blue lines, and purple versus pink lines). At the intermediate and fastest $v$, the more stratified domains ($\varepsilon = 0.006$, blue and pink lines) have a higher upper bound of risk. In the case of the intermediate $v$, differences in stratification result in differences in exceeding the $10^{-4}$ remediation action level. Aside from $v$ and $\varepsilon$, perhaps the most controlling risk variable for the continuous source with LD ensembles is differences in the sorption scenario. The upper bounds of *Kin1* (dashed lines), $v = 0.001$ [m d$^{-1}$] and $v = 0.01$ [m d$^{-1}$] ensembles are significantly higher than those of their LEA counterparts (solid lines). This result confirms the importance of the LD-kinetic sorption feedback shown in Figures 4b, 4d, and 4f and demonstrates it as a governing process in accurately calculating risk. $Da_{Global}$ does not accurately characterize these ensembles that reflect disequilibrium conditions.

[44] Unlike $v = 0.001$[m d$^{-1}$] and $v = 0.01$ [m d$^{-1}$], the upper bounds of risk for the $v = 0.1$ [m d$^{-1}$] ensembles (purple and pink lines) are similar for both sorption scenarios. When compared to the less stratified domain with infinite *Pe*, (Figure 9a, $\varepsilon = 0.1$, purple lines) the ensemble statistics of the finite *Pe* ensembles (Figure 9b, $\varepsilon = 0.1$, purple lines) mirror each other. Stratified domains with infinite *Pe* (Figure 9a, $\varepsilon = 0.006$, pink lines) and finite *Pe* (Figure 9b, $\varepsilon = 0.006$, pink lines) both demonstrate large distributions in risk, but the mean of the finite *Pe* ensembles are larger than the near-zero (less than $10^{-10}$) mean risk estimates of the infinite *Pe* ensembles. In other words, while the uncertainty associated with both scenarios is large, it is more certain that an aquifer modeled with LD will yield cancer risk above the *de minimis* RAL. This comparison for continuous source ensembles illustrates the importance of accurately representing small-scale reactions such as kinetic sorption and LD, especially for $v = 0.001$

[m $d^{-1}$] and $v = 0.01$ [m $d^{-1}$] ensembles. Because the source is continuous and therefore the environmental concentration ($\overline{C}$) dependence on time should be small to nonexistent (see Appendix B1), these results exemplify the strong dependence of small-scale reactions in risk assessment. A second finding of importance is the invariance of LD and kinetic sorption with high-$v$ ensembles (especially the less stratified aquifer, purple lines, where equilibrium conditions exist), suggesting a tipping point in variable dominance when calculating risk.

#### 4.5.2. Pulse Source Risk

[45] Figure 10a shows the probability of risk for a pulse source with infinite *Pe* whereas Figure 10b shows the probability of risk for a finite *Pe*. For each *Pe* scenario, all ensembles are dissimilar, and disequilibrium conditions always exist. Thus, the use of $Da_{Global}$ for any of these ensembles would be a poor predictor of equilibrium conditions. Unlike the risk results given a continuous source (section 4.5.1), changes in each variable (i.e., $v$, $\varepsilon$, *Pe*, and sorption scenario) show sensitivity to risk. In general, upper bounds of risk increase with (1) an increase in $v$, (2) a decrease in $\varepsilon$, and (3) LEA ensembles in comparison to *Kin1* ensembles. Again, an exception persists in the case of the less stratified aquifer, $v = 0.1$ [m $d^{-1}$] case (Figures 10a and 10b, purple lines) where risk decreases at $v = 0.1$ [m $d^{-1}$]. While trends 1 and 2 are consistent with the results for the continuous source (Figure 9), trend 3 is the opposite. The time dependence associated with the pulse source and with sorption kinetics diminishes the overall effect of the peak concentration (see Figure 5), resulting in lower probabilities of cancer risk in comparison to LEA ensembles (Figure 10, differences in dashed versus solid lines). Because mass is conserved in the simulation, the decreased peak concentration results in a smearing of the breakthrough curve and an increasing tail. We previously noted greater $R_{eff,Kin1}$ ensemble variances when compared to the ensemble variances of $C_{pk,Kin}/C_{pk,tracer}$ (Figure 7) and that the additive LD-kinetic sorption effect yielded the highest change in effective retardations (see $\Delta R_{eff,Tail}$ statistics, Table 4). It is important to distinguish here that the risk simulations are directly dependent on the value of $\overline{C}$ (see discussion in Appendix B), and do not reflect the variance in effective retardations directly. For all $v$, the effect of LD decreases both LEA and *Kin1* risk upper bound values. Differences in $\varepsilon$ are present for finite and infinite *Pe*, consistent with the results from the $R_{eff,Disp}$ metric (Figure 8 and Table 4). These effects are small in comparison to the additive LD-kinetic sorption effect observed in the continuous source analysis.

## 5. Conclusions

[46] The effects of kinetically sorbing solutes in stratified aquifers were studied to assess realistic far-field groundwater contamination scenarios. This study focused on cases where variations in sedimentology and stratigraphy are dominant factors in determining contaminant flow and transport and ultimately risk assessment. Contamination of a potable drinking water aquifer with mobile arsenic was used as an example case study to investigate the effect of differing hydrologic parameters such as: pulse versus continuous sources, differences in the anisotropy ratio, mean groundwater velocity, kinetic or LEA sorption, and with and without the inclusion of LD. An investigation of potential interplay (positive or negative feedbacks) between multiple hydrogeologic parameters was conducted for both kinetic and LEA ensembles to assess the validity and predictability of LEA through comparisons of stochastic ensembles. A number of new metrics were utilized to assess flow and transport behavior, and finally carcinogenic human health risk was used as an endpoint of comparison by utilizing a risk methodology previously developed [*Maxwell and Kastenberg*, 1999; *Siirila et al.*, 2012] where risk is calculated using a nested Monte Carlo approach. Principal findings include:

[47] 1. Using representative realizations of each ensemble, large distribution of $Da_{Local}$ were calculated, and could be directly related to the distribution of $v$ within the domain. For all ensembles, a portion of the $Da_{Local}$ distribution falls within tracer, kinetic, and equilibrium regimes. In contrast, all calculations of $Da_{Global}$ yielded equilibrium conditions. For the hydrologic scenarios considered here, peak concentration and risk results show $Da_{Global}$ is only an accurate predictor given a continuous source without LD. For all pulse sources (with and without LD), the peak concentrations and risk results show $Da_{Global}$ is inaccurate predictor of equilibrium conditions.

[48] 2. Parametric sensitivity to LD is sensitive to the degree of aquifer stratification. To isolate the effect of LD alone, a comparison of tracer (i.e., nonsorbing solutes) is conducted with finite and infinite *Pe*. Results show the driver in the effective retardation of dispersion is the difference in stratification, where the less stratified domain exhibits little difference between finite and infinite *Pe*, and the stratified domain exhibits nonnegligible differences between finite and infinite *Pe*. These differences are apparent in two subsets of results, where the solute is either moved from a zone of high $K$ to low $K$, and the plume is retarded, or vice versa when the plume is accelerated. This finding suggests the inclusion of LD (even if only on the mm scale) will cause an effective retardation of the overall plume, particularly for highly stratified domains. While it has been previously been shown that the effect of LD affect the second moment of the plume [*Dagan and Fiori*, 1997; *Fiori et al.*, 2002; *Fiorotto and Caroni*, 2002; *Bellin et al.*, 2004], we show the effect of LD either retards or excels the first moment of the plume, represented here as the peak time and concentration, a phenomena which has yet to be reported in the literature.

[49] 3. An additive, or positive feedback, between LD and kinetic sorption was found to be a controlling process in accurately simulating solute behavior by adding an effective tailing behavior as high as approximately 30 times that of a LEA solute without LD. We speculate that the effect is controlled at the high-low-$K$ interface, where the induced cell-based mixing creates particle jumps from interconnected high-$K$ regions into regions of low $K$ and vice versa. The time dependence associated with kinetic sorption into and out of solution is magnified with LD, yielding solute behavior unlike that of equilibrium simulations when the effective retardation of kinetics is much less than $R$. Here we show the LD-kinetic sorption effect retards the first moment of the plume, a second interdependence phenomenon not previously documented. This proposed

conceptual model is valid given with respect to a number of presented results including peak concentration distributions, effective retardations, and the variance of the connectivity indicator.

[50] 4. Parametric sensitivity to aquifer channeling is sensitive to the degree of aquifer stratification. While the mean connectivity is independent of $\varepsilon$, the variance in connectivity is highly dependent on $\varepsilon$ where connectivity is highly variable for stratified ensembles and more uniform for less stratified ensembles. Either very fast (interconnected high-$K$ zones) or slow flow (interconnected low-$K$ zones) paths dominate flow fields of highly anisotropic media. Connectivity variance is the greatest for ensembles including LD and kinetic ensembles, further promoting the results discussed in principal finding 3.

[51] 5. The magnitude and distribution of carcinogenic human health risk is highly dependent on the source term (pulse versus continuous). Equilibrium conditions exist for the continuous source without LD and only for high mean groundwater velocities with LD. All other hydrologic conditions for the continuous source, and for all conditions for the pulse source display disequilibrium conditions. While the cancer risk estimates given the pulse source are small in comparison to the continuous source, the demonstrated parametric sensitivity is substantial, suggesting the feedbacks between processes such as LD and kinetic sorption are significant and should not be neglected in risk analysis modeling or in groundwater solute transport problems.

[52] 6. In general, upper bounds of carcinogenic risk increase with (1) an increase in $v$ and (2) an increase in aquifer stratification. The additive LD-kinetic sorption effect relates to a higher upper bound of risk for the continuous source and a lower upper bound of risk for the pulse source. This opposition is due to the increased time dependence in the pulse source scenario, and therefore the increased tailing effect.

[53] These results suggest small-scale mechanisms such as LD and kinetic sorption are controlling of not only solute transport processes but also human health risk assessment. Implications of this study are relevant in upcoming technological challenges in groundwater contaminant transport with relevance in human health risk assessments.

[54] A limitation of this analysis is the investigation of other intermediate spatial scales such as the length of the well screen, the well capture zone, and also sensitivity in the size of the source relative to the integral scale. Recent work has begun to address this problem, and would be complimentary to this work [*de Barros and Nowak*, 2010]. Although the magnitude of the horizontal integral scale was investigated in this work, the model of spatial persistence of $Y$ was not explored for sensitivity. Because many models of heterogeneity have been developed and compared [e.g., *Lee et al.*, 2007], another next step in this analysis would be a comparison of these models of $Y$. Second, while parametric uncertainty was a central focus of this study, model uncertainty was not addressed. Full reactive transport models (i.e., including nonlinear reactions such as dissolution and precipitation) are computationally expensive, and at this discretization and spatial extent, are virtually impossible except with a very large number of processors (i.e., on the order of millions) and with long computational times [*Hammond and Lichtner*, 2010]. Future analyses include sensitivity at intermediate scales and also an intermodel comparison of different techniques to address the flow and transport feedbacks addressed here as a method to bound model uncertainty.

## Appendix A: Flow and Transport

[55] Far-field aquifer flow is simulated using the parallel, three-dimensional groundwater model ParFlow, [*Ashby and Falgout*, 1996; *Jones and Woodward*, 2001; *Kollet and Maxwell*, 2006] utilizing a very efficient multigrid preconditioned conjugate gradient solver. Perturbation theory is used to characterize $Y = \ln(K)$ as a mean and perturbation [*Rubin*, 2003]:

$$\begin{aligned} Y &= \langle Y \rangle + y' \\ \langle y' \rangle &= 0 \\ \langle y' \rangle^2 &= \sigma^2_{\ln(K)} \end{aligned}, \tag{A1}$$

where bracketed terms, $\langle\,\rangle$, denote the mean or expected value and $y'$ is the perturbation from the mean $Y$. Three-dimensional, spatially correlated random fields of $K$ are internally generated in ParFlow using the turning bands algorithm [*Tompson et al.*, 1989]. Steady state groundwater flow is described by:

$$\nabla \cdot q = -\nabla \cdot (K \nabla h) = 0, \tag{A2}$$

where $h$ [m] is the hydraulic head and $q$ [m d$^{-1}$] is the Darcy flux. Local groundwater velocity ($v$) [m d$^{-1}$] is defined by Darcy's law as:

$$v = \frac{-K \nabla h}{\theta}. \tag{A3}$$

[56] Varying conditions of solute transport are simulated using the Lagrangian particle tracking model SLIM-FAST [*Maxwell and Kastenberg*, 1999; *Maxwell et al.*, 2007; *Maxwell*, 2010] where solute transport is governed by the advection-dispersion equation [*Fetter*, 1999]:

$$\frac{\partial C}{\partial t} = D_L \frac{\partial^2 C}{\partial x^2} + D_T \frac{\partial^2 C}{\partial y^2} - v \frac{\partial C}{\partial x} - \frac{\rho_b \partial C^*}{\theta \partial t} - i, \tag{A4}$$

where $D_L$ [m$^2$ d$^{-1}$] and $D_T$ [m$^2$ d$^{-1}$] are the small-scale (local), hydrodynamic longitudinal and transverse dispersion coefficients (respectively), and $i$ is a source or sink [mg m$^{-3}$ d$^{-1}$]. Contaminant mass balance is accounted via:

$$\begin{aligned} \frac{\partial}{\partial t}\left(\theta(C + C^*)\right) &= \nabla \cdot (\vec{\theta D} \cdot \nabla C) - \nabla \cdot (\theta v C) \\ &\quad - C \sum\nolimits_w Q_w \delta(x - x_w)\delta(y - y_w)\delta(z - z_w), \end{aligned} \tag{A5}$$

where $Q_w$ [m$^3$ d$^{-1}$] is the pumping rate of well $w$ situated at ($x_w$, $y_w$, $z_w$) and $\vec{D}$ is the hydrodynamic dispersion tensor defined as:

$$\vec{D} = (\alpha_T |v| + \hat{D})\breve{I} + (\alpha_L - \alpha_T)\frac{vv}{|v|}, \tag{A6}$$

where $\alpha_L$ [m] and $\alpha_T$ [m] are longitudinal and transverse dynamic dispersivity (respectively), $\hat{D}$ [$m^2$ $d^{-1}$] is the effective molecular diffusivity, and $\breve{I}$ is the unit vector. This case study utilizes $\alpha_L$ and $\alpha_T$ parameters (see Table 1) to account for LD. A BiLinear velocity interpolation, was found to be the most accurate method of solving for the advection-correction and random-walk dispersion terms in particle displacement [*LaBolle et al.*, 1996], and is implemented here. A full description of the equations used in the particle-tracking model and further information on model validation is described by *Maxwell* [2010].

## Appendix B: Human Health Risk

[57] Adverse health effects to potentially exposed individuals from a contaminant are quantified using a calculation of an individual's exposure in conjunction with a toxicity dose. Risk is discussed in terms of a probability of carcinogenic risk, although the increased risk of other noncancer adverse health effects can easily be quantified using a similar methodology via the hazard index [*Siirila et al.*, 2012]. The equations presented here are generally based on those described in the US EPA Risk Assessment Guidance for Superfund (*RAGS*) Volumes I and III [*U.S.EPA*, 1989, 2001], as well as other studies presented in the recent literature [*Bogen and Spear*, 1987; *Mckone and Bogen*, 1991, 1992; *Maxwell et al.*, 1998; *Maxwell and Kastenberg*, 1999; *Maxwell et al.*, 1999; *Maxwell et al.*, 2008]. All calculations are based on a baseline assessment of risk, where remediation action is not considered. Monitoring or remediation is not the purpose of this study but can easily be implemented in the methodology presented here.

## Appendix B1. Exposure

[58] Two exposure pathways are considered: ingestion of tap water and dermal sorption through skin in washing, bathing, etc. Arsenic is not a volatile contaminant according to *RAGS Volume 1, Part B* [*U.S.EPA*, 1991], thus the contribution from the inhalation pathway (i.e., vapor via showering, washing, etc.) will therefore be much smaller than the other pathways and is not modeled in this case study. Exposure from the ingestion and dermal pathways are defined by the average daily dose ($ADD_{ingestion}$, $ADD_{dermal}$, respectively) [$mg_{As}$ $kg^{-1}$ $d^{-1}$]:

$$ADD_{ingestion} = \overline{C}\left(\frac{IR}{BW}\right)\frac{ED \cdot EF}{AT}, \tag{B1}$$

$$ADD_{dermal} = \overline{C}\left(\frac{SA}{BW}\right)\frac{ED \cdot EF}{AT}K_p \cdot f_{skin} \cdot ED_{shower}CF, \tag{B2}$$

where $\overline{C}$ [mg $L^{-1}$] is the maximum average well concentration of arsenic recorded over the exposure duration ($ED$) [yrs], $IN/BW$ [L kg $d^{-1}$] is the ingestion rate of water per unit body weight, $AT$ [day] is the averaging time or expected lifetime, $EF$ [d $yr^{-1}$] is the standard exposure frequency, $SA/BW$ [$m^2$ $kg^{-1}$] is the skin surface area in contact with water per unit body weight, $K_p$ [m $h^{-1}$] is the dermal permeability coefficient of the compound in water, $f_{skin}$ [-] is the fraction of skin in contact with water, $ED_{shower}$ [h $d^{-1}$] is the shower exposure duration, and $CF$ is the unit conversion factor ($1 \times 10^{-3}$ L $m^{-3}$). Standard values suggested by *RAGS* for $ED$, $EF$, and $AT$ are listed in Table 2. Equations (B1) and (B2) are used to quantify risk for chronic exposure (7–70 years) opposed to subchronic exposure (2 weeks to 7 years) [*U.S.EPA*, 1989].

[59] Accurately quantifying the value of $\overline{C}$ is one of the overall objectives of this paper, and is the motivation for performing a parametric sensitivity analysis on the flow and transport parameters in the case study. Evaluating $\overline{C}$ is significant since concentration breakthrough curves for each well effluent correspond to the concentrations that will eventually reach the individual. $\overline{C}$ is linearly related to exposure (see equations (B1) and (B2)), therefore augmenting the need to accurately quantify the range of expected $\overline{C}$ values within an ensemble. $\overline{C}$ is calculated at each well ($w$), and is averaged over the $ED$:

$$\overline{C}_w = MAX\left[\frac{\sum_{t}^{t+ED} c_w(t)}{ED}\right]_{t=0}^{t=\infty}, \tag{B3}$$

where $c_w$ [mg $L^{-1}$] is the concentration at that well as a function of time ($t$). Continuous sources will reach a maximum, steady state concentration that is constant over time (and therefore a constant, maximum values over the $ED$). Time-dependent parameters are therefore not expected to change after the maximum concentration is reached for contamination scenarios with a continuous source. Pulse sources utilize the maximum of a running average of the entire well breakthrough curve over the $ED$ [e.g., see *Maxwell et al.*, 1998, Figure 1]. Sensitivity between $\overline{C}_w$ and $ED$ has been investigated for $ED$ ranging between 5 and 70 years, where smaller $ED$ values are associated with higher $\overline{C}_w$ characterization [*Maxwell et al.*, 2008]. However, because the $ED$ value appears in the calculation for exposure (i.e., equations (B1) and (B2)), smaller averaging times also result less exposure and therefore in a smaller probability of risk.

## Appendix B2. Carcinogenic Toxicity

[60] Pathway specific carcinogenic toxicity values are used to calculate an increased probability of an individual developing cancer over a lifetime, generally under the assumption that a linear relationship exists between exposure to the contaminant and the risk of cancer. However, the effect of nonlinear relationships [e.g., *U.S.EPA*, 2005] have been briefly explored in the context of groundwater risk assessment [*de Barros et al.*, 2009]. For all carcinogens, any level of exposure will cause cellular proliferation leading to a clinical state of disease with a finite probability of an adverse health effect occurring, regardless of the exposure dose. An extrapolation procedure is used for low-level doses via a dose response curve, sometimes yielding high levels of uncertainty at low-exposure doses [*Cothern et al.*, 1986]. While some studies suggest the linear extrapolation is an appropriate assumption for most carcinogens [*Guess et al.*, 1977], it should be noted that this procedure is somewhat controversial [*Guess et al.*, 1977; *Bogen and Gold*, 1997] especially if the studied exposure dose is a nonhuman species [*Wogan et al.*, 2004; *Trosko and Upham*, 2005].

[61] The primary parameter that quantifies carcinogenic toxicity is the pathway specific cancer potency factor (*CPF*) [kg d mg$^{-1}$]. A tabulated value from the US EPA Integrated Risk Information System (IRIS) database for the arsenic ingestion pathway ($CPF_{ingestion}$) is used. As suggested by the US EPA [*U.S.EPA*, 2004], toxicity values for the dermal pathway are derived by an extrapolation of oral toxicity values. This relationship is defined by utilizing percentages of gastrointestinal absorption ($ABS_{GI}$ [-]) and is established on the theory that ingestion is based on the quantity of the contaminant administered and therefore directly relational to the quantity of the contaminant absorbed:

$$\frac{Risk_{dermal}}{Risk_{ingestion}} \propto \frac{1}{ABS_{GI}}, \tag{B4}$$

where the cancer potency factor for the dermal pathway ($CPF_{dermal}$) [kg d mg$^{-1}$] is defined by:

$$CPF_{dermal} = \frac{CPF_{ingestion}}{ABS_{GI}}. \tag{B5}$$

For those contaminants whose $ABS_{GI}$ are undocumented or are not scientifically defensible, a (conservative) value of 100% is suggested. An arsenic $ABS_{GI}$ value of 95% is used here based on the work of *Bettley and O'Shea* [1975]. Toxicity values used in this case study are listed in Table 2.

## Appendix B3. Probability of Risk

[62] Human health risk of an individual incurring cancer over a lifetime of exposure is calculated by combining the exposure and toxicity parameters (discussed in sections B1 and B2, respectively) through pathway $i$:

$$Risk = 1 - \exp^{-CPF_i \times ADD_i \times f_i^*}, \tag{B6}$$

where $f_i^*$ is a pathway and contaminant specific metabolized fraction of contaminant, developed using a pharmacokinetic (PBPK) model to account for decay products of the contaminant that may be present once consumed [*Mckone and Bogen*, 1992]. Here we assume a value of $f_i^* = 1$ for arsenic. Overall risk is then quantified as the summation for $n$ pathways:

$$Risk = \sum_{i=1}^{i=n} Risk_i. \tag{B7}$$

Remediation Action Levels (RALs) are defined as the probability risk value at which remediation is warranted to prevent cancer. RAL values typically fall between $10^{-4}$ [-] and $10^{-6}$. Remediation is often warranted if risk exceeds the upper level ($10^{-4}$ [-]), corresponding to a probability of 1 in 10,000 individuals incurring cancer. Remediation is often not warranted if risk does not exceed the lower level ($10^{-6}$ [-]), corresponding to a probability of 1 in 1,000,000 individuals incurring cancer. The latter is often referred to as the *de minimis* action level, or negligible risk that is too small to be of societal concern and is otherwise "virtually safe."

## Appendix B4. Uncertainty and Variability

[63] Risk of an individual incurring cancer over a lifetime is treated using a probabilistic risk assessment (PRA), explicitly differentiating between uncertain and variable parameters. Here we define uncertainty as a lack of knowledge or measurement error, primarily associated with environmental parameters (i.e., hydrologic flow field, primarily $K$). In contrast, we define variability as natural diversity, often associated with interindividual differences (i.e., physiological and exposure differences between an adult and a child). For the sake of simplicity, we choose to distinguish parameters as either uncertain or variable, although in reality some parameters may be both (for example, variability in body weight and uncertainty in the measurement accuracy of the scale). Another distinction is that uncertainty can be reduced, whereas variability can only be further characterized [*Morgan et al.*, 1990; *Mckone and Bogen*, 1992; *Finley et al.*, 1994; *Maxwell et al.*, 1998; *Maxwell and Kastenberg*, 1999; *Maxwell et al.*, 1999; *Daniels et al.*, 2000]. Here we adopt terminology introduced previously [e.g., *Maxwell et al.*, 1998] and term fractiles of variability as subpopulations within the overall population, where the 95th and/or 99th fractiles of variability are often used to describe the maximally exposed (i.e., most sensitive to contamination) individual. We discuss percentiles of uncertainty as scientific confidence, where the 50th percentile of uncertainty is often used to describe the "best scientific guess". Benefits of calculating risk in terms of joint uncertainty and variability (JUV) include the following:

[64] 1. A tool for decision makers to generate relationships that differentiate between individual sensitivity, risk, and scientific uncertainty.

[65] 2. The ability to predict a change (or potential decrease) in individual risk as a function of reduction of uncertainty or measurement error.

[66] A nested (or two-step) Monte Carlo approach is used to address JUV. Discrete distributions are utilized for uncertain (environmental well concentrations, $\overline{C}$) and variable (individual exposure variables related to physiology or time, see e.g., equations (B1) and (B2)) parameters. For one sampling of the uncertain distribution (one $\overline{C}$ value given one realization of flow and transport), a complete sampling of all variability parameters distributions (exposure for all individuals within a population) is conducted. This process can be conceptualized as an inner (variable) and outer (uncertain loop), where a complete sampling of the inner loop is repeated for each realization of the outer loop [see e.g., *Maxwell et al.*, 1999, Plate 1; *Siirila et al.*, 2012, Figure 2]. This process yields a 2-D surface of risk, where fractiles of variability and percentiles of uncertainty can easily be discerned. Slices along this surface, usually at fractiles of interest such as the 50th fractile (average exposed individual) or 99th fractile (maximally exposed individual) provide meaningful comparisons of differences in individual sensitivity and cumulative scientific uncertainty.

## Notation

| | |
|---|---|
| $K$ | hydraulic conductivity, m d$^{-1}$. |
| $x_d$, $y_d$, $z_d$ | domain size in the $x$, $y$, and $z$ directions. |
| $Y$ | natural logarithm of hydraulic conductivity, m d$^{-1}$. |

$K_g$ geometric mean of hydraulic conductivity, m d$^{-1}$.
$\sigma_Y^2$ variance of hydraulic conductivity.
$\xi$ separation distance, m.
$\lambda_h$ horizontal correlation length, m.
$\lambda_v$ vertical correlation length, m.
$\varepsilon$ anisotropy ratio.
$v$ local groundwater velocity.
$K_D$ partition coefficient, L kg$^{-1}$.
$C$ aqueous concentration in solution, mg kg$^{-1}$.
$C^*$ sorbed concentration in the solid phase, mg m$^{-3}$.
$k_f$ forward sorption rate, L d$^{-1}$.
$k_r$ reverse sorption rate, kg d$^{-1}$.
$R$ solute retardation.
$R_{LEA}$ solute retardation from equilibrium sorption.
$R_{kin}$ solute retardation from kinetic sorption.
$\theta$ porosity.
$\rho_b$ bulk density of the porous medium, kg m$^{-3}$.
$t_{adv}$ advection time, day.
$t_{aq}$ aqueous time, day.
$t_s$ sorbed time, day.
$RN$ random number from a normal distribution.
$t_{particle}$ particle time, day.
$p$ particle number.
$Pe$ nondimensional Péclet number.
$dx$ cell size parallel to groundwater flow, m.
$\vec{v}$ cell based local velocity vector, m d$^{-1}$.
$v_x$, $v_y$, $v_z$ directional components of $\vec{v}$ [m d$^{-1}$].
$Da_{Local}$ local Damköhler number.
$Da_{Global}$ global Damköhler number.
$t_{pk}$ peak well breakthrough time, day.
$C_{pk}/C_0$ normalized peak well breakthrough concentration.
$nw$ number of wells.
$nr$ number of realizations.
$R_{eff,LEA}$ effective retardation from equilibrium sorption.
$R_{eff,kin}$ effective retardation from kinetic sorption.
$R_{eff,Disp}$ effective retardation from local dispersion.
$\Delta R_{eff,Tail}$ effective retardation from local dispersion and kinetic sorption.
$CI$ connectivity indicator.
$t_5$ time at which 5% of particle mass is present at the well, day.
$t_{50}$ time at which 50% of particle mass is present at the well, day.
$\Delta x$, $\Delta y$, $\Delta z$ cell discretization in the x, y, and z directions, m.
$nx$, $ny$, $nz$ number of cells in the x, y, and z directions.
$t_{arr,v}$ dimensionless arrival time.
$Q_{regional,v}$ regional volumetric flux, m$^3$ d$^{-1}$.
$v_{particle}$ particle velocity, m d$^{-1}$.
$\overline{\Delta R_{eff,Tail}}$ mean effective retardation of tailing.
$\sigma_{\Delta R_{eff,Tail}}$ standard deviation of effective retardation of tailing.
$\overline{CI}$ average connectivity indicator.
$\sigma_{CI}$ standard deviation of the connectivity indicator.
$ADD_{ingestion}$ exposure from ingestion, mg$_{As}$ kg$^{-1}$ d$^{-1}$.
$ADD_{dermal}$ exposure from dermal sorption, mg$_{As}$ kg$^{-1}$ d$^{-1}$.
$\overline{C}$ maximum average well concentration, mg L$^{-1}$.
$ED$ exposure duration, years.
$IN/BW$ ingestion rate of water per unit body weight, L kg d$^{-1}$.
$AT$ averaging time, day.
$EF$ exposure frequency, d yr$^{-1}$.
$SA/BW$ skin surface area in contact with water per unit body weight, m$^2$ kg$^{-1}$.
$K_p$ dermal permeability coefficient in water, m h$^{-1}$.
$f_{skin}$ fraction of skin in contact with water.
$ED_{shower}$ shower exposure duration, h d$^{-1}$.
$CF$ conversion factor, L m$^{-3}$.
$c_w$ concentration at the well as a function of time, mg L$^{-1}$.
$ABS_{GI}$ gastrointenstinal absorption.
$CPF$ cancer potency factor, kg d mg$^{-1}$.
$CPF_{ingestion}$ cancer potency factor for the ingestion pathway, kg d mg$^{-1}$.
$CPF_{dermal}$ cancer potency factor for the dermal pathway, kg d mg$^{-1}$.
$f^*$ metabolized fraction of contaminant.
$y'$ perturbation of $Y$, m d$^{-1}$.
$h$ hydraulic head, m.
$q$ Darcy flux, m d$^{-1}$.
$D_L$ local hydrodynamic longitudinal dispersion coefficient, m$^2$ d$^{-1}$.
$D_T$ local hydrodynamic transverse dispersion coefficient, m$^2$ d$^{-1}$.

[67] **Acknowledgments.** Funding for this work was provided by DOE NETL grant DE-FE0002059 and EPA STAR grant RD-83438701-0. This research was supported in part by the Golden Energy Computing Organization at the CO School of Mines using resources acquired with financial assistance from the National Science Foundation and the National Renewable Energy Laboratory. This research has been supported in part by a grant from the US Environmental Protection Agency's Science to Achieve Results (STAR) program. Although the research described in the article has been funded wholly or in part by the US Environmental Protection Agency's STAR program through grant RD-83438701-0, it has not been subjected to any EPA review and therefore does not necessarily reflect the views of the Agency, and no official endorsement should be inferred. We wish to thank the associate editor and three anonymous reviewers for improving the quality and clarity of this work.

## References

Ababou, R., D. McLaughlin, L. Gelhar, and A. Tompson (1989), Numerical simulation of three-dimensional saturated flow in randomly heterogeneous porous media, *Transp. Porous Media*, *4*(6), 549.

Andričević, R., and V. Cvetkovíc (1996), Evaluation of risk from contaminants migrating by groundwater, *Water Resour. Res.*, *32*(3), 611.

Andričević, R., and E. Foufoula-Georgiou (1991), Modeling kinetic non-equilibrium using the first two moments of the residence time distribution, *Stoch. Hydrol. Hydraul.*, *5*(2), 155.

Andričević, R., J. Daniels, and R. Jacobson (1994), Radionuclide migration using a travel time transport approach and its application in risk analysis, *J. Hydrol.*, *163*(1–2), 125.

Ashby, S., and R. Falgout (1996), A parallel multigrid preconditioned conjugate gradient algorithm for groundwater flow simulations, *Nucl. Sci. Eng.*, *124*(1), 145.

Bahr, J. M., and J. Rubin (1987), Direct comparison of kinetic and local equilibrium formulations for solute transport affected by surface reactions, *Water Resour. Res.*, *23*(3), 438.

Bellin, A., and Y. Rubin (2004), On the use of peak concentration arrival times for the inference of hydrogeological parameters, *Water Resour. Res.*, *40*, W07401, doi:10.1029/2003WR002179.

Bellin, A., and D. Tonina (2007), Probability density function of non-reactive solute concentration in heterogeneous porous formations, *J. Contam. Hydrol.*, *94*(1–2), 109.

Bellin, A., A. Lawrence, and Y. Rubin (2004), Models of sub-grid variability in numerical simulations of solute transport in heterogeneous porous formations: Three-dimensional flow and effect of pore-scale dispersion, *Stoch. Environ. Res. Risk Assess.*, *18*(1), 31.

Benekos, I., C. Shoemaker, and J. Stedinger (2007), Probabilistic risk and uncertainty analysis for bioremediation of four chlorinated ethenes in groundwater, *Stoch. Environ. Res. Risk Assess.*, *21*(4), 375.

Berg, M., H. Tran, T. Nguyen, H. Pham, R. Schertenleib, and W. Giger (2001), Arsenic contamination of groundwater and drinking water in Vietnam: A human health threat, *Environ. Sci. Technol.*, *35*(13), 2621.

Bettley, F., and J. O'Shea (1975), The absorption of arsenic and its relation to carcinoma, *Br. J. Dermatol.*, *92*(5), 563.

Bianchi, M., C. Zheng, C. Wilson, G. R. Tick, G. Liu, and S. M. Gorelick (2011), Spatial connectivity in a highly heterogeneous aquifer: From cores to preferential flow paths, *Water Resour. Res.*, *47*, W05524, doi:10.1029/2009WR008966.

Bogen, K., and L. Gold (1997), Trichloroethylene cancer risk: Simplified calculation of PBPK-based MCLs for cytotoxic end points* 1, *Regul. Toxicol. Pharm.*, *25*(1), 26.

Bogen, K. T., and R. C. Spear (1987), Integrating uncertainty and interindividual variability in environmental risk assessment, *Risk Anal.*, *7*(4), 427.

Bolster, D., and D. Tartakovsky (2008), Probabilistic risk analysis of building contamination, *Indoor Air*, *18*(5), 351.

Bolster, D., M. Barahona, M. Dentz, D. Fernandez-Garcia, X. Sanchez-Vila, P. Trinchero, C. Valhondo, and D. M. Tartakovsky (2009), Probabilistic risk analysis of groundwater remediation strategies, *Water Resour. Res.*, *45*, W06413, doi:10.1029/2008WR007551.

Brusseau, M. L., and R. Srivastava (1997), Nonideal transport of reactive solutes in heterogeneous porous media 2. Quantitative analysis of the Borden natural-gradient field experiment, *J. Contam. Hydrol.*, *28*(1–2), 115.

Chen, C., C. Chen, M. Wu, and T. Kuo (1992), Cancer potential in liver, lung, bladder and kidney due to ingested inorganic arsenic in drinking water, *Br. J. Cancer*, *66*(5), 888.

Chin, D. A., and T. Wang (1992), An investigation of the validity of first-order stochastic dispersion theories in isotropie porous media, *Water Resour. Res.*, *28*(6), 1531.

Christakos, G. (1992), *Random Field Models in Earth Sciences*, Academic Press, San Diego, Calif.

Cothern, C. R., W. A. Coniglio, and W. L. Marcus (1986), Development of quantitative estimates of uncertainty in environmental risk assessments when the scientific data base is inadequate, *Environ. Int.*, *12*(6), 643.

Cvetkovic, V., and G. Dagan (1994), Transport of kinetically sorbing solute by steady random velocity in heterogeneous porous formations, *J. Fluid. Mech.*, *265*, 189.

Cvetkovic, V., and A. Shapiro (1990), Mass arrival of sorptive solute in heterogeneous porous media, *Water Resour. Res.*, *26*(9), 2057.

Dagan, G. (1982), Stochastic modeling of groundwater flow by unconditional and conditional probabilities: 2. The solute transport, *Water Resour. Res.*, *18*(4), 835.

Dagan, G., and V. Cvetkovic (1993), Spatial moments of a kinetically sorbing solute plume in a heterogeneous aquifer, *Water Resour. Res.*, *29*(12), 4053.

Dagan, G., and A. Fiori (1997), The influence of pore-scale dispersion on concentration statistical moments in transport through heterogeneous aquifers, *Water Resour. Res.*, *33*(7), 1595.

Daniels, J., K. Bogen, and L. Hall (2000), Analysis of uncertainty and variability in exposure to characterize risk: Case study involving trichloroethylene groundwater contamination at Beale Air Force Base in California, *Water Air Soil Pollut.*, *123*(1), 273.

Darland, J. E., and W. P. Inskeep (1997), Effects of pore water velocity on the transport of arsenate, *Environ. Sci. Technol.*, *31*(3), 704.

de Barros, F. P. J., and W. Nowak (2010), On the link between contaminant source release conditions and plume prediction uncertainty, *J. Contam. Hydrol.*, *116*(1), 24.

de Barros, F., and Y. Rubin (2008), A risk-driven approach for subsurface site characterization, *Water Resour. Res.*, *44*, W01414, doi:10.1029/2007WR006081.

de Barros, F. P. J., Y. Rubin, and R. M. Maxwell (2009), The concept of comparative information yield curves and its application to risk-based site characterization, *Water Resour. Res.*, *45*, W06401, doi:10.1029/2008WR007324.

Espinoza, C., and A. J. Valocchi (1997), Stochastic analysis of one-dimensional transport of kinetically adsorbing solutes in chemically heterogeneous aquifers, *Water Resour. Res.*, *33*(11), 2429.

Fernandez-Garcia, D., D. Bolster, X. Sanchez-Vila, and D. M. Tartakovsky (2012), A Bayesian approach to integrate temporal data into probabilistic risk analysis of monitored NAPL remediation, *Adv. Water Resour.*, *36*, 108–120, doi:10.1016/j.advwatres.2011.07.001.

Fetter, C. (1999), *Contaminant Hydrogeology*, Prentice Hall, Upper Saddle River, N. J.

Finley, B., D. Proctor, P. Scott, N. Harrington, D. Paustenbach, and P. Price (1994), Recommended distributions for exposure factors frequently used in health risk assessment, *Risk Anal.*, *14*(4), 533.

Fiori, A. (1996), Finite Peclet extensions of Dagan's solutions to transport in anisotropic heterogeneous formations, *Water Resour. Res.*, *32*(1), 193.

Fiori, A., and A. Bellin (1999), Non-ergodic transport of kinetically sorbing solutes, *J. Contam. Hydrol.*, *40*(3), 201.

Fiori, A., S. Berglund, V. Cvetkovic, and G. Dagan (2002), A first-order analysis of solute flux statistics in aquifers: The combined effect of pore-scale dispersion, sampling, and linear sorption kinetics, *Water Resour. Res.*, *38*(8), 1137, doi:10.1029/2001WR000678.

Fiorotto, V., and E. Caroni (2002), Solute concentration statistics in heterogeneous aquifers for finite Peclet values, *Transp. Porous Media*, *48*(3), 331.

Green, C. T., J. K. Böhlke, B. A. Bekins, and S. P. Phillips (2010), Mixing effects on apparent reaction rates and isotope fractionation during denitrification in a heterogeneous aquifer, *Water Resour. Res.*, *46*, W08525, doi:10.1029/2009WR008903.

Guess, H., K. Crump, and R. Peto (1977), Uncertainty estimates for low-dose-rate extrapolations of animal carcinogenicity data, *Cancer Re.*, *37*(10), 3475.

Guo, H. R., H. S. Chiang, H. Hu, S. R. Lipsitz, and R. R. Monson (1997), Arsenic in drinking water and incidence of urinary cancers, *Epidemiology*, *8*, 545.

Hammond, G. E., and P. C. Lichtner (2010), Field-scale model for the natural attenuation of uranium at the Hanford 300 Area using high-performance computing, *Water Resour. Res. 46*, W09527, doi:10.1029/2009WR008819.

Hassan, A. E., R. Andričević, and V. Cvetkovic (2001), Computational issues in the determination of solute discharge moments and implications for comparison to analytical solutions, *Adv. Water Resour.*, *24*(6), 607.

Indelman, P., and G. Dagan (1999), Solute transport in divergent radial flow through heterogeneous porous media, *J. Fluid. Mech.*, *384*, 159.

Jennings, A. A. (1984), Instantaneous equilibrium approximation analysis, *J. Hydraul. Eng.*, *110*, 1700.

Jones, J. E., and C. S. Woodward (2001), Newton-Krylov-multigrid solvers for large-scale, highly heterogeneous, variably saturated flow problems, *Adv. Water Resour.*, *24*(7), 763.

Keller, R. A., and J. C. Giddings (1960), Multiple zones and spots in chromatography, *J. Chromatogr. A*, *3*, 205.

Knudby, C., and J. S. Carrera (2005), On the relationship between indicators of geostatistical, flow and transport connectivity, *Adv. Water Resour.*, *28*(4), 405.

Kollet, S. J., and R. M. Maxwell (2006), Integrated surface-groundwater flow modeling: A free-surface overland flow boundary condition in a parallel groundwater flow model, *Adv. Water Resour.*, *29*(7), 945.

LaBolle, E. M., G. E. Fogg, and A. F. B. Tompson (1996), Random-walk simulation of transport in heterogeneous porous media: Local mass-conservation problem and implementation methods, *Water Resour. Res.*, *32*(3), 583.

LaBolle, E. M., G. E. Fogg, and J. B. Eweis (2006), Diffusive fractionation of 3H and 3He in groundwater and its impact on groundwater age estimates, *Water Resour. Res.*, *42*, W07202, doi:10.1029/2005WR004756.

LaBolle, E. M., G. E. Fogg, J. B. Eweis, J. Gravner, and D. G. Leaist (2008), Isotopic fractionation by diffusion in groundwater, *Water Resour. Res.*, *44*, W07405, doi:10.1029/2006WR005264.

Lee, S.-Y., S. F. Carle, and G. E. Fogg (2007), Geologic heterogeneity and a comparison of two geostatistical models: Sequential Gaussian and transition probability-based geostatistical simulation, *Adv. Water Resour.*, *30*(9), 1914.

Maxwell, R. M. (2010), *SLIM-FAST: A User's Manual*, vol. 4, International Ground Water Modeling Center (IGWMC), Golden, CO.

Maxwell, R. M., and W. E. Kastenberg (1999), Stochastic environmental risk analysis: An integrated methodology for predicting cancer risk from contaminated groundwater, *Stoch. Environ. Res. Risk Assess.*, *13*(1–2), 27.

Maxwell, R. M., S. D. Pelmulder, A. F. B. Tompson, and W. E. Kastenberg (1998), On the development of a new methodology for groundwater-driven health risk assessment, *Water Resour. Res.*, *34*(4), 833.

Maxwell, R. M., W. E. Kastenberg, and Y. Rubin (1999), A methodology to integrate site characterization information into groundwater-driven health risk assessment, *Water Resour. Res.*, *35*(9), 2841.

Maxwell, R. M., C. Welty, and R. W. Harvey (2007), Revisiting the Cape Cod bacteria injection experiment using a stochastic modeling approach, *Environ. Sci. Technol.*, *41*(15), 5548.

Maxwell, R., S. Carle, and A. Tompson (2008), Contamination, risk, and heterogeneity: On the effectiveness of aquifer remediation, *Environ. Geol.*, *54*(8), 1771.

Mckone, T. E., and K. T. Bogen (1991), Predicting the uncertainties in risk assessment: A California groundwater case-study, *Environ. Sci. Technol.*, *25*(10), 1674.

Mckone, T. E., and K. T. Bogen (1992), Uncertainties in health-risk assessment: An integrated case-study based on tetrachloroethylene in California groundwater, *Regul. Toxicol. Pharm.*, *15*(1), 86.

Michalak, A. M., and P. K. Kitanidis (2000), Macroscopic behavior and random-walk particle tracking of kinetically sorbing solutes, *Water Resour. Res.*, *36*(8), 2133.

Miralles-Wilhelm, F., and L. Gelhar (1996), Stochastic analysis of sorption macrokinetics in heterogeneous aquifers, *Water Resour. Res.*, *32*(6), 1541.

Mishra, A., A. Gutjahr, and H. Rajaram (1999), Transport with spatially variable kinetic sorption: recursion formulation, *Adv. Water Resour.*, *22*(5), 549.

Morgan, M., M. Henrion, and M. Small (1990), *Uncertainty: A Guide to Dealing With Uncertainty in Quantitative Risk and Policy Analysis*, Cambridge Univ. Press, New York.

Nickson, R., J. McArthur, W. Burgess, K. Ahmed, P. Ravenscroft, and M. Rahman (1998), Arsenic poisoning of Bangladesh groundwater, *Nature*, *395*(6700), 338.

Ogola, J., W. Mitullah, and M. Omulo (2002), Impact of gold mining on the environment and human health: A case study in the Migori gold belt, Kenya, *Environ. Geochem. Health*, *24*(2), 141.

Pickens, J., R. Jackson, K. Inch, and W. Merritt (1981), Measurement of distribution coefficients using a radial injection dual-tracer test, *Water Resour. Res.*, *17*(3), 529.

Quinodoz, H. N. A. M., and A. J. Valocchi (1993), Stochastic analysis of the transport of kinetically sorbing solutes in aquifers with randomly heterogeneous hydraulic conductivity, *Water Resour. Res.*, *29*(9), 3227.

Rehfeldt, K. R., J. M. Boggs, and L. W. Gelhar (1992), Field-study of dispersion in a heterogeneous aquifer. 3. Geostatistical analysis of hydraulic conductivity, *Water Resour. Res.*, *28*(12), 3309.

Roberts, P. V., M. N. Goltz, and D. M. Mackay (1986), A natural gradient experiment on solute transport in a sand aquifer: 3. Retardation estimates and mass balances for organic solutes, *Water Resour. Res.*, *22*(13), 2047.

Rubin, Y. (2003), *Applied Stochastic Hydrogeology*, Oxford Univ. Press, New York.

Salandin, P., and V. Fiorotto (1998), Solute transport in highly heterogeneous aquifers, *Water Resour. Res.*, *34*(5), 949.

Sánchez-Vila, X., and J. Solís-Delfín (1999), Solute transport in heterogeneous media: The impact of anisotropy and non-ergodicity in risk assessment, *Stoch. Environ. Res. Risk Assess.*, *13*(5), 365.

Selroos, J.-O. (1995), Temporal moments for nonergodic solute transport in heterogeneous aquifers, *Water Resour. Res.*, *31*(7), 1705.

Selroos, J. O., and V. Cvetkovic (1992), Modeling solute advection coupled with sorption kinetics in heterogeneous formations, *Water Resour. Res.*, *28*(5), 1271.

Selroos, J. O., and V. Cvetkovic (1994), Mass flux statistics of kinetically sorbing solute in heterogeneous aquifers: Analytical solution and comparison with simulations, *Water Resour. Res.*, *30*(1), 63.

Siirila, E. R., A. K. Navarre-Sitchler, R. M. Maxwell, and J. E. McCray (2012), A quantitative methodology to assess the risks to human health from CO2 leakage into groundwater, *Adv. Water Resour.*, *36*, 146.

Smalley, J. B., B. S. Minsker, and D. E. Goldberg (2000), Risk-based in situ bioremediation design using a noisy genetic algorithm, *Water Resour. Res.*, *36*(10), 3043.

Smith, A. H., C. Hopenhayn-Rich, M. N. Bates, H. M. Goeden, I. Hertz-Picciotto, H. M. Duggan, R. Wood, M. J. Kosnett, and M. T. Smith (1992), Cancer risks from arsenic in drinking water, *Environ. Health Perspectives*, *97*, 259.

Smith, E., and R. Naidu (2009), Chemistry of inorganic arsenic in soils: Kinetics of arsenic adsorption–desorption, *Environ. Geochem. Health*, *31*, 49.

Springer, R. K. (1991), Application of an improved slug test analysis to the large-scale characterization of heterogeneity in a cape cod aquifer, Master of Science in Civil Engineering, 162 pp., Dep. of Civ. Eng., Mass. Inst. of Technol., Cambridge, Mass.

Tartakovsky, A. M., and S. P. Neuman (2008), Effects of Peclet number on pore-scale mixing and channeling of a tracer and on directional advective porosity, *Geophys. Res. Lett.*, *35*, L21401, doi:10.1029/2008GL035895.

Tartakovsky, D. M. (2007), Probabilistic risk analysis in subsurface hydrology, *Geophys. Res. Lett.*, *34*, L05404, doi:10.1029/2007GL029245.

Tompson, A. F. B., and D. E. Dougherty (1992), Particle-grid methods for reacting flows in porous media with application to Fisher's equation, *Appl. Math. Modell.*, *16*(7), 374.

Tompson, A. F. B., R. Ababou, and L. W. Gelhar (1989), Implementation of the three-dimensional turning bands random field generator, *Water Resour. Res.*, *25*(10), 2227.

Trosko, J. E., and B. L. Upham (2005), The emperor wears no clothes in the field of carcinogen risk assessment: Ignored concepts in cancer risk assessment, *Mutagenesis*, *20*(2), 81.

United States Environmental Protection Agency (1989), Risk assessment guidance for superfund, in *Human Health Evaluation Manual, Part A*, Vol. 1, 284 pp., Office of Emergency and Remedial Response, U.S. Environmental Protection Agency, Washington, D.C.

United States Environmental Protection Agency (1991), Risk assessment guidance for superfund, in *Human Health Evaluation Manual, Part B*, Vol. 1, 61 pp., Office of Emergency and Remedial Response, U.S. Environmental Protection Agency, Washington, D.C.

United States Environmental Protection Agency (2001), Risk assessment guidance for superfund, in *Process for Conducting Probabilistic Risk Assessment Part A*, Vol. 3, 385 pp., Office of Emergency and Remedial Response, U.S. Environmental Protection Agency, Washington, D.C.

United States Environmental Protection Agency (2004), Risk assessment guidance for superfund, in *Human Health Evaluation Manual, Part E*, Vol. I, 156 pp., Office of Emergency and Remedial Response, U.S. Environmental Protection Agency, Washington, D.C.

United States Environmental Protection Agency (2005), Guidelines for carcinogen risk assessment, *Rep. EPA/630/P-03/001F*, Washington, D.C.

Valocchi, A. (1985), Validity of the local equilibrium assumption for modeling sorbing solute transport through homogeneous soils, *Water Resour. Res.*, *21*(6), 808.

Valocchi, A. J. (1988), Theoretical analysis of deviations from local equilibrium during sorbing solute transport through idealized stratified aquifers, *J. Contam. Hydrol.*, *2*(3), 191.

Valocchi, A. J. (1989), Spatial moment analysis of the transport of kinetically adsorbing solutes through stratified aquifers, *Water Resour. Res.*, *25*(2), 273.

Valocchi, A. J., and H. A. M. Quinodoz (1989), Application of the random walk method to simulate the transport of kinetically adsorbing solutes, in *Proceedings of the Symposuium held during the Third IAHS Scientific Assembly*, pp. 35–42, Baltimore, Md., publ. 185, Int. Assoc. Hydrolog. Sci., Wallingford, U.K.

Wogan, G. N., S. S. Hecht, J. S. Felton, A. H. Conney, and L. A. Loeb (2004), Environmental and chemical carcinogenesis, *Semin. Cancer Biol.*, *14*(6), 473.

Yu, W. H., C. M. Harvey, and C. F. Harvey (2003), Arsenic in groundwater in Bangladesh: A geostatistical and epidemiological framework for evaluating health effects and potential remedies, *Water Resour. Res.*, *39*(6), 1146, doi:10.1029/2002WR001327.

R. M. Maxwell and E. R. Siirila, Hydrologic Science and Engineering Program, Colorado School of Mines, 1500 Illinois St., Golden, CO 80401, USA. (esiirila@mymail.mines.edu)